Identification of factors that prevent ribosome stalling during early elongation

Authors: Hye-Rim Hong[1], Cassidy R. Prince[1], Letian Wu[1], Heather A. Feaga[1]*

Affiliations:

[1] Department of Microbiology, Cornell University, Ithaca, NY 14853

* Corresponding author haf54@cornell.edu

Keywords: ribosome quality control; ABCFs; Uup; EttA; translation initiation; EF-P; *Bacillus anthracis*; *Bacillus subtilis*

Abstract

Protein synthesis is catalyzed by the ribosome and a host of highly conserved elongation factors. Most elongation factors that are conserved in all domains of life are essential, such as EF-Tu (e/aEF1A) and EF-G (e/aEF2). In contrast, the universally conserved elongation factor P (EF-P/eIF5A) is essential in eukaryotes but is dispensable in most bacteria. EF-P prevents ribosome stalling at difficult-to translate sequences, especially polyprolines. Since *efp* deletion phenotypes range from modest to lethal in different bacterial species, we hypothesized that some bacteria encode an uncharacterized elongation factor with compensatory functions. To identify this factor, we used Tn-seq to screen for genes that are essential in the absence of EF-P in *Bacillus subtilis*. This screen identified YfmR, a member of the ABCF family of ATPases, as a translation factor that is essential when *efp* is deleted. We find that depleting YfmR from Δ*efp* cells decreases actively translating ribosomes and increases free ribosomal subunits bound to initiator tRNA, suggesting that ribosomes stall in early elongation. We also find that deleting *efp* from the spore-forming pathogen *Bacillus anthracis* causes a severe survival defect in liquid culture and in the presence of macrophages. *B. anthracis* Δ*efp* also does not produce detectable spores. We find that heterologous expression of *B. subtilis* YfmR in *B. anthracis* Δ*efp* cells partially rescues the severe growth and sporulation defects of this mutant. Our results therefore identify YfmR as an important translation factor that becomes essential in the absence of EF-P, and suggest that the essential function of YfmR and EF-P is to assist translation during early elongation.

Significance

Translation is one of the most ancient and energetically demanding process that occurs in the cell. Ribosomes constitute more than 60% of cellular mass in actively growing cells, and ribosomes are a major target of antimicrobials and chemotherapeutics. Here, we report evidence that both EF-P and the uncharacterized protein YfmR are important for early translation elongation

in bacteria, and that this activity is essential. YfmR is a member of the ABCF family of ATPases whose role in translation is only beginning to be understood. Given the broad distribution of ABCFs from bacteria to fungi, we expect our results to have implications for understanding the crucial first steps of translation elongation in diverse organisms.

Introduction

Ribosomes decode mRNAs to produce proteins (1). Translation initiates when an mRNA, along with IF1, IF2, and IF3 bind the small (30S) ribosomal subunit. IF2 and IF3 ensure that a special tRNA charged with formyl-methionine ($tRNA^{fMet}$) is positioned at the P-site during initiation (2-4). After IF3 dissociation, the large (50S) subunit joins to form the 70S. After dissociation of IF1 and IF2, the ribosome is ready for the first charged tRNA to be delivered into the A-site by EF-Tu (5, 6). Once the incoming tRNA is accommodated, the large subunit catalyzes peptide bond formation at a region called the peptidyl-transferase center (PTC) (7-9). After transpeptidation, the ribosome is advanced one codon by EF-G (10). Elongation then proceeds at a rate of approximately 15 codons sec^{-1}(11) and terminates when the ribosome reaches a stop codon (12).

Many highly conserved translation factors participate directly in decoding and elongation, while others interact with the ribosome to maintain translation speed and fidelity (13). Some translation factors were present in the last universal common ancestor (LUCA) and are essential in all domains of life, including IF2 (e/aIF5B in), EF-Tu (e/aEF1A), and EF-G (e/aEF2) (14, 15). Others, such as EF-P (e/aIF5a in eukaryotes and archaea), are essential in some species but not others (16, 17). eIF5a is essential in *Saccharomyces cerevisiae* (18) and in *Drosophila melanogaster* (19, 20) due to its role as a general translation factor that participates in both elongation and termination (21-24). EF-P is essential in some bacterial species, such as *Acinetobacter baumannii* (25) *Neisseria meningitidis* (26), and *Mycobacterium tuberculosis* (27), but is dispensable in others, such as *Escherichia coli* (28-30) and *Bacillus subtilis* (28, 31-34).

EF-P in bacteria promotes transpeptidation between amino acids that are poor donors and acceptors of peptide bonds (29, 35-41). In particular, polyproline tracts pose a special challenge for ribosomes (37, 42-46), since proline has a cyclic structure that introduces a turn in the polypeptide and therefore a poor geometry for peptide bond formation (47). Early biochemical and structural characterizations of EF-P also indicate that EF-P can stimulate formation of the first peptide bond, but this activity has not been detected *in vivo*. Purified EF-P stimulates peptide

bond formation between fMet-Lys, fMet-Leu, and fMet-Gly (18), but not fMet-Phe (18, 39). Ribosome profiling studies have not detected ribosome stalling at initiation, but have confirmed that EF-P prevents ribosome stalling at polyprolines *in vivo* (33, 34, 48).

Since early biochemical characterizations of purified EF-P suggest it can stimulate formation of the first peptide bond, we hypothesized that it may have this role *in vivo* as well, but that this function is masked by another protein. Furthermore, Δ*efp* phenotypes among bacterial species range from modest to lethal, further suggesting that some bacteria encode an additional elongation factor that has a function similar to EF-P. Therefore, we used Tn-seq to identify genes that are essential in *B. subtilis* in the absence of EF-P and that play a critical role in translation. Our screen uncovered *yfmR*, which encodes an ABCF family ATPase, as a gene that is essential in the absence of EF-P. YfmR depletion by CRISPRi in Δ*efp* cells decreased actively translating ribosomes and increased the abundance of free ribosomal subunits, suggesting that these cells may have a defect either during or shortly after translation initiation. To monitor early elongation, we compared levels of initiator $tRNA^{fMet}$ associated with ribosomal subunits, since ribosomes that stall at early elongation will have $tRNA^{fMet}$ bound to the small subunit. When we depleted YfmR from Δ*efp* cells, initiator tRNAs associated with the free 30S small subunit and 70S ribosomes increased. Additionally, we demonstrate that EF-P is essential for sporulation and optimal growth in *Bacillus anthracis*, and that heterologous expression of YfmR from *B. subtilis* can partially rescue these phenotypes. Single deletion of *efp* from *B. anthracis* mimics depletion of YfmR in *B. subtilis* Δ*efp* and also leads to increased association of $tRNA^{fMet}$ with the 30S small ribosomal subunit and with 70S ribosomes. Our work therefore establishes a role for both EF-P and YfmR during early elongation *in vivo*.

Results

B. anthracis exhibits severe growth and sporulation defects when *efp* is deleted.

The essentiality of *efp* in some pathogenic bacteria suggests it could be a good antibiotic target. To test the requirement of EF-P in a pathogenic Gram-positive bacterium, we constructed an in-frame unmarked *efp* deletion in *Bacillus anthracis* Sterne. *B. anthracis* Sterne Δ*efp* had a severe growth defect at 37˚C (Fig 1). Wild-type cells had a growth rate of 0.8 ± 0.01 hour $^{-1}$, whereas Δ*efp* cells had growth rate of 0.5 ± 0.01 hour $^{-1}$ (37.5% reduction in growth rate). The growth defect was even more severe at 30˚C, a temperature that intensifies translation phenotypes (49-51). A single chromosomally integrated copy of *efp* expressed under the control of an IPTG inducible promoter restored the growth rate at both temperatures. *B. anthracis* Δ*efp* cells produced no observable spores after 24 hours of growth in sporulation media (Fig 1B) and were also defective in survival in the presence of macrophages (Fig S1), suggesting that EF-P may also be important for *B. anthracis* persistence in the environment and its pathogenesis.

The ABCF ATPase YfmR is synthetic lethal with EF-P

Despite its important role in translation, EF-P is dispensable in many bacteria, suggesting that some species encode proteins with compensatory functions. Ribosome profiling in *B. subtilis* shows that the Δ*efp* strain has increased stalling at polyproline motifs and (33, 34) confirming its major role in translation polyprolines in this species. *B. anthracis* and *B. subtilis* encode similar numbers of poly-proline motifs (30 and 33 respectively), but unexpectedly *B. anthracis* Δ*efp* exhibits phenotypes that are markedly more severe than *B. subtilis* Δ*efp* (Fig. 1). Therefore, we hypothesized that *B. subtilis* encodes additional factors that compensate for loss of EF-P.

To identify genes that are essential in the absence of EF-P, we performed transposon mutagenesis followed by Illumina sequencing (Tn-seq) to identify genes that have fewer insertions in the Δ*efp* background compared to wild type. We transformed *B. subtilis* genomic DNA that had

been transposon mutagenized *in vitro* (52) into *B. subtilis* wild-type and Δ*efp* cells. We pooled libraries of >450,000 colonies from each strain, then mapped and tallied the transposon insertion sites.

One of the genes with the most significant difference in transposon insertions between the two strains was *yfmR*, which encodes a poorly characterized ABCF ATPase in the Uup subfamily (15). *B. subtilis* Δ*efp* cells had a 20-fold reduction in insertions in this gene compared to wild type, suggesting *yfmR* may be essential when *efp* is absent (Fig 2B). To test this, we first measured transformation efficiency of Δ*yfmR::kan*^{R} genomic DNA into a Δ*efp* background. Δ*spoIIE::kan*^{R} genomic DNA (carrying a deletion of the non-essential *spoIIE* gene) was used as a positive control. While the positive control plate had >1,000 colonies, only 2 colonies formed on the plate where Δ*efp* had been transformed with Δ*yfmR::kan*^{R}, and PCR revealed that both colonies maintained a wild-type copy of *yfmR* (suggesting the *kan*^{R} allele had inserted into a different locus). Next, we used CRISPR interference (53) to deplete YfmR from Δ*efp* cells by co-expressing deactivated Cas9 (dCas9) and a guide RNA targeting *yfmR (*P_{xyl} – dCas9 P_{veg} – sgRNA^{yfmR}) (Fig 2C). Co-expressing dCas9 with sgRNA^{yfmR} in wild-type cells did not impact colony formation (Fig 2D). However, when dCas9 with sgRNA^{yfmR} were co-expressed in Δ*efp* cells, these cells failed to form colonies at both 30 ˚C and 37 ˚C (Fig 2D), demonstrating that *yfmR* and *efp* are a synthetic lethal pair in *B. subtilis*.

YfmR is not important for preventing ribosome stalling at polyproline tracts

EF-P binds to the ribosomal E-site and assists translation of poly-proline tracts and other difficult-to-translate sequences (29, 36-39). All ABCFs investigated to date bind the E-site (54, 55). Therefore, we hypothesized that YfmR may play a role in rescuing ribosomes stalled at prolines and be functionally redundant with EF-P. To investigate this, we designed an N-terminally Flag-tagged reporter to quantify polyproline-induced stalling. The coding sequence of *rfp* (not including the stop codon) was fused to the coding sequence of *cfp* with a 5-proline motif in

between them (Fig 3A). The resulting reporter construct was placed under the control of an IPTG promoter and integrated as a single copy into the wild-type and Δ*efp B. subtilis* chromosome. Stalling at the polyproline motif results in a peptide that is approximately ½ the size of the full-length protein. In Δ*efp* cells we observed a significant amount of stalling on this motif as expected (34.9 ± 2.6% stalling during mid-log phase and 42 ± 9.3% in late log phase) (Fig 3B). In contrast, no stalling was observed in wild-type or in Δ*yfmR* cells. *B. anthracis* Δ*efp* cells exhibited similar levels of stalling on a reporter with a polyproline motif (31.7 ± 6.5%) (Fig S2). Since we did not detect ribosome stalling in Δ*yfmR* we hypothesized that it may have a role in translation that does not involve facilitating translation of polyproline tracts.

Depleting YfmR from Δ*efp* cells reduces actively translating ribosomes and increases unengaged ribosomal subunits

To investigate whether YfmR impacts translation, we used sucrose density gradient ultracentrifugation to characterize the ribosomes of *B. subtilis* Δ*efp* cells when YfmR was depleted by CRISPRi. Cultures of *B. subtilis* wild type, Δ*efp* and Δ*efp* P_{xyl} – dCas9 P_{veg} – $sgRNA^{yfmR}$ (Δ*efp* YfmR depletion strain) were grown overnight without xylose. Cultures were inoculated into fresh LB and xylose was added to 2.5% to induce dCas9+$sgRNA^{yfmR}$. After ~3 hours of dCas9+$sgRNA^{yfmR}$ induction cells were lysed and ribosomes were separated on a 10%-40% sucrose gradient. Area under the curve for 30S, 50S, 70S and polysomes peaks was quantified and used to determine relative abundance of each ribosome species (Fig S3).

efp deletion from *B. subtilis* did not significantly impact the distribution of ribosome species on the gradients compared to wild type (Fig 4A, Fig S3). However, when YfmR was depleted from Δ*efp* cells by CRISPRi, 70S and polysomes decreased by 34.2 ± 6.1 % compared to wild type (Fig S3). Ribosomes in polysome populations are actively translating, while some 70S are actively translating and others are empty subunits that have become coupled in the gradient (56).

Therefore, the significant decrease in 70S and polysomes indicates that there is a severe translation defect when YfmR is depleted from Δ*efp* cells.

In contrast to *B. subtilis*, Δ*efp* single deletion from *B. anthracis* caused a severe decrease in actively translating ribosomes, and increased free 30S and 50S subunits (Fig 4B). 70S and polysomes decreased by 37.6 ± 3.4 % in *B. anthracis* Δ*efp* compared to wild type (Fig S3). *B. anthracis* Δ*efp* ribosome gradients resemble *B. subtilis* Δ*efp* when YfmR is depleted. These data suggest that the YfmR homolog in *B. anthracis* is not as active as heterologously expressed *B. subtilis* YfmR or not expressed as strongly.

We also observed a 100S ribosomal peak in log-phase *B. anthracis*, similar to what has been reported for other Gram-positive species like *Staphylococcus aureus* (57, 58). We confirmed that these 100S ribosomes were HPF-bound hibernating ribosomes by probing gradient fractions with an antibody raised against HPF (59) and by deleting *hpf* and confirming that this peak was absent in the Δ*hpf* strain (Fig S4).

Higher levels of initiator tRNAs remain bound to ribosomes in the absence of EF-P and YfmR

Free 30S and 50S subunits increased in both *B. anthracis* Δ*efp* and in *B. subtilis* Δ*efp* co-expressing dCas9 and sgRNA^{yfmR} (Fig. 4). YfmR is a member of the Uup subfamily of ABCF ATPases. All ABCFs investigated to date bind the ribosomal E-site (55). *E. coli* Uup contacts tRNA^{fMet} in the P-site and positions it to promote a favorable geometry for peptide bond formation (55). Although Uup did not stimulate tripeptide synthesis between fMet-Phe-Lys, it may stimulate peptide bond formation between other amino acids (60). Therefore, we hypothesized that a translation failure was occurring early in translation, likely at the first steps of protein synthesis. To monitor early elongation, we assayed levels of initiator tRNA^{fMet} associated with ribosomal subunits since initiating ribosomes will have tRNA^{fMet} bound to them. We fractionated 30S, 50S, 70S, and polysomes by sucrose density gradient ultracentrifugation and precipitated total RNA

from these peaks. Normalized rRNA was separated on a TBE urea gel and probed with a $tRNA^{fMet}$ specific oligonucleotide. The ratio of $tRNA^{fMet}$ to 16S rRNA was then quantified to determine levels of $tRNA^{fMet}$ association with the small subunit in the various strains. Initiator $tRNA^{fMet}$ associated with the 30S small subunits significantly increased when YfmR was depleted in *B. subtilis* Δ*efp* cells compared to wild type ($p = 0.0031$), indicating that translation stalls after initiation in this mutant (Fig 4C). Initiator $tRNA^{fMet}$ also increased in the 70S ribosomes in *B. subtilis* Δ*efp* expressing $sgRNA^{yfmR}$, though not as severely as for the 30S subunits ($p = 0.02$). Higher levels of initiator $tRNA^{fMet}$ were also detected with the 30S small subunits of *B. anthracis* Δ*efp* compared to wild type ($p = 0.0045$) and in the 70S ribosomes ($p = 0.04$) (Fig 4D). These results suggest that ribosomes stall in early elongation in *B. anthracis* Δ*efp* and in *B. subtilis* Δ*efp* when YfmR is depleted.

B. subtilis YfmR partially rescues the *B. anthracis* Δ*efp* growth and sporulation defects

The combination of Δ*efp* and CRISPRi depletion of YfmR is lethal to *B. subtilis*, while *B. anthracis* has a severe but non-lethal phenotype when *efp* is deleted. *B. anthracis* encodes a YfmR homolog (WP_000783212.1) that shares 57% amino acid sequence identity with *B. subtilis* YfmR. Structural modeling with AlphaFold (61) of *B. subtilis* and *B. anthracis* YfmR shows that they are structurally similar (Fig 5A). However, the phenotypes of *B. subtilis* Δ*efp* with YfmR depletion are similar to the *B. anthracis* Δ*efp* single deletion. Both have fewer actively translating ribosomes and higher levels of initiating tRNAs bound to free 30S ribosomal subunits suggesting that they both experience stalling shortly after initiation (Fig 4). To test whether *B. subtilis* YfmR could complement the *B. anthracis* growth defect we expressed IPTG-inducible YfmR as a single copy integrated into the *B. anthracis* genome (Fig 5B). Expression of *B. subtilis* YfmR partially, but significantly, rescued the growth defect of *B. anthracis* Δ*efp* at both 30˚C ($p = 0.04$) and 37˚C ($p = 0.01$). Induction of *B. subtilis* YfmR also partially rescued the *B. anthracis* Δ*efp* sporulation

defect and increased sporulation to detectable levels (Fig 5C). These data suggest that *B. anthracis* YfmR is not as effective as YfmR from *B. subtilis*, or that it is poorly expressed.

YfmR is a homolog of Uup but is more similar to EttA in the PTC-contacting domain.

B. subtilis YfmR contains the coiled coil extension at its C-terminus that is a hallmark of the Uup subfamily of ABCFs (Fig 6A). However, YfmR has comparable sequence identity to both EttA (36%) and Uup (35%). EttA has a prominent role in translation initiation (54, 62), while Uup from *E. coli* failed to stimulate tripeptide bond formation *in vitro* (60) and has been proposed to play a role in ribosome assembly (15). ABCFs bind the ribosomal E-site and their specific functions are determined by variations in length and amino acid composition of two alpha-helical extensions known as the arm and the inter-ABC-domain linker (also called the PtIM) (55). The arm interacts with the L1 stalk, while the linker/PtIM reaches up to the peptidyl-transferase-center. EttA's linker domain (PtIM domain, residues 242-322) makes specific contacts with $tRNA^{fMet}$ (Fig 6B) and discriminates between $tRNA^{fMet}$ and elongator tRNAs to promote a favorable geometry for peptide bond formation specifically during initiation (54, 55, 60, 62). Since YfmR depletion in the Δ*efp* background stalled the ribosome with $tRNA^{fMet}$ bound (Fig 4C), we hypothesized that YfmR is performing a function similar to EttA. Therefore, we examined the individual domains of YfmR and compared the arm, linker/PtIM, and C-terminal domains of YfmR to those of Uup and EttA (Fig 6C). The YfmR PtIM domain had 34% sequence identity with the PtIM domain of EttA, but only 24% sequence identity with the PtIM domain of Uup. The arm domain of YfmR, which should contact the L1 stalk, is also more similar to EttA (27%) than to Uup (23%). Next, we compared ABCFs of *B. subtilis*, *B. anthracis*, and *E. coli* to examine their likely evolutionary history. Consistent with previous reports, we observed that EttA and Uup share a common ancestor exclusive of the other ABCFs with a maximum likelihood bootstrap percentage of >90% (Fig 6D). YfmR from *B. subtilis* and from *B. anthracis* clustered with EttA instead of Uup, but with

lower certainty (66% MLB). The observation that YfmR is more similar to EttA, particularly in the PtIM/linker region that interacts with $tRNA^{fMet}$, further supports a role for YfmR in stimulating the formation of the first peptide bond.

Discussion

Here we show that EF-P and YfmR prevent ribosome stalling during early elongation and that this activity is essential, since deleting both *efp* and *yfmR* is lethal (Fig 2, Fig 4). Depleting YfmR from Δ*efp* cells increased free 30S and 50S ribosomal subunits and caused a substantial increase in $tRNA^{fMet}$ associated with the free 30S subunits relative to wild type ($p = 0.0031$) (Fig 4). $tRNA^{fMet}$ associated with the 70S ribosome also increased, though to a lesser extent than was associated with the free 30S subunits (Fig 4). These data support a model in which initiating ribosomes fail to form either the first or second peptide bond in the absence of YfmR and EF-P, then separate into independent subunits due to the absence of the stabilizing force of the peptide in the exit tunnel. This model is consistent with recent studies showing that errors within the first 15 codons cause dissociation of the 70S elongation complex (63).

YfmR is an ABCF protein that is a member of the Uup subfamily (Fig 6) (64). The role of ABCFs in translation is only beginning to be understood. There are 45 distinct subfamilies of ABCFs and bacteria encode an average of 4 ABCFs per genome (64). *B. subtilis* encodes 4 ABCFs (yfmR, ydiF, ykpA, and yfmM). Of these, only *yfmR* was a significant hit in our Tn-seq screen. YfmR is classified in the Uup subfamily due to a 91 amino acid extension at its C-terminus, but is annotated as EttA by NCBI since it has marginally higher overall sequence identity with EttA (36%) than with Uup (35%). Both EttA and Uup from *E. coli* bind the ribosomal E-site and encode a linker that contains the P-site tRNA interacting motif (PtIM), and both were recently shown to bind the E-site and promote a favorable catalytic geometry for peptide bond formation (55). Although *E. coli* Uup did not stimulate translation of a tripeptide motif (fMet-Phe-Lys) *in vitro* (60), we think it is likely to stimulate early elongation of other peptides such as fMet-Lys, fMet-

Leu, or fMet-Gly as has been shown for EF-P (35). Crucially, we also detected $tRNA^{fMet}$ in the polysomes of all our strains, but $tRNA^{fMet}$ showed no increase in Δ*efp* or in Δefp $sgRNA^{yfmR}$ cells, suggesting that initiation in polysomes does not have a dependence on EF-P or YfmR. mRNAs being translated in polysomes have stronger Shine-Delgarno sequences whereas those associated with 70S monosomes have weaker SD sequences (56). Strength of the SD may therefore be an important factor in determining the necessity of EF-P and YfmR for early elongation.

Additional lines of evidence support a role for both EF-P and YfmR in assisting early elongation. First, EF-P prevents frameshifting at noncognate proline codons, particularly when they occur at the second codon of the message (41, 56, 65). These data suggest both that EF-P can be accommodated in the E-site shortly after initiation, and that peptide bond formation between the first and second amino acids is uniquely challenging (41). Second, parallels between EF-P and EttA have been previously speculated since $tRNA^{fMet}$ and $tRNA^{Pro}$ are the only tRNAs that contain a unique CpU bulge in the D-loop (54). Since YfmR is most similar to EttA in the PtIM region, YfmR may make similar contacts to this unique feature of $tRNA^{fMet}$ and $tRNA^{Pro}$. Although we did not observe increased stalling at a motif containing 5 proline codons in the Δ*yfmR* single deletion, future experiments will test whether YfmR depletion in the Δ*efp* background does cause increased stalling at polyprolines. These experiments will determine whether there is additional functional overlap between YfmR and EF-P. Finally, super-resolution fluorescence tracking of EF-P in *E. coli* demonstrates that EF-P binds the ribosomal E-site during at least 25% of all elongation events, further suggesting a broader role for EF-P in elongation (66).

Deleting *efp* from *B. anthracis* caused phenotypes that were more severe than *B. subtilis* Δ*efp* (Fig 1) and which were similar to *B. subtilis* Δ*efp* expressing dCas9 + $sgRNA^{yfmR}$ (Fig 4). *B. anthracis* Δ*efp* had a severely reduced growth rate (Fig 1) as well as higher levels of free 30S and 50S subunits (Fig 4B), and increased $tRNA^{fMet}$ associated with 30S and 70S (Fig 4D). *B. anthracis* Sterne encodes a YfmR homolog (WP_000783212.1) that is 57% identical to *B. subtilis* YfmR.

Expressing a single copy of YfmR from a weak *hyperspank* promoter partially rescued the growth defect of *B. anthracis* Δ*efp* (Fig 5B). Therefore, it is likely that *B. anthracis* YfmR is less active in promoting elongation, or is weakly expressed.

Finally, our work gives important insights into the physiological role of EF-P and YfmR in *B. subtilis* and *B. anthracis*, two Gram-positive spore formers that are relevant to biotechnology and human health. Deleting *efp* from *B. anthracis* completely abolished sporulation, and therefore severely diminished survival of these cells within 24 hours in liquid culture (Fig 1B). *B. anthracis* Δ*efp* was also significantly more sensitive to killing by macrophages (Fig S1), suggesting that EF-P may be a good target for antibiotics in Gram positive species in addition to Gram-negatives (27, 30). Lastly, the finding that *yfmR* and *efp* are a synthetically lethal pair in Gram-positive species suggests that the ABCF protein family should be prioritized as targets for antibiotic development. Since these proteins are ATPases, it is likely that these proteins are highly druggable.

Materials and Methods

Strains and media

All strains were derived from *B. subtilis* 168 *trpC2* and *B. anthracis* Sterne 34F2 and are listed in Table 1. *B. subtilis* and *B. anthracis* were grown in Lysogeny Broth (67) media at 30˚C and 37˚C as indicated. *B. anthracis* strains were cultured in Brain Heart Infusion (BHI) for conjugation. *E. coli* strains were cultured in LB. Antibiotics were used at final concentrations of 100 µg/mL ampicillin (68), and 20 µg/mL kanamycin (18), 100 µg/mL spectinomycin (Spec) and 1x MLS (1 µg/mL erythromycin and 25 µg/mL lincomycin).

Construction of *B. anthracis* Δ*efp*

A DNA fragment (Twist Biosciences) containing 700-bp regions flanking the *efp* open reading frame along with 30 bp of homology to pRP1028 at the 5' and 3' ends was cloned into pRP1028 (69) at the BamHI restriction site by Gibson assembly (70) to create plasmid pHRH28. pHRH28 was conjugated into *B. anthracis* Sterne by tri-parental mating as described previously (69). Briefly, the strain harboring the donor plasmid was mixed with helper plasmid pSS1827 (71) and recipient *B. anthracis* Sterne by mixing on BHI plates and incubating at room temperature overnight. The mixture was scraped and spread onto BHI agar media supplemented with 250 µg/mL spectinomycin and 60 units of Polymyxin B. Integrants were restruck on BHI plates containing spectinomycin. A second tri-parental mating was then performed to transform the integrants with plasmid pRP1099 harboring the SceI nuclease. Donor, helper, and recipient strains were mixed and the mating proceeded at 37˚C for 8 hours. Since the previously integrated donor plasmid pRP1028 contains a SceI endonuclease target site, introducing the new donor plasmid pRP1099 carrying the SceI endonuclease facilitates *B. anthracis* chromosome recombination. Spectinomycin sensitive colonies were screened for *efp* deletion by PCR using primers HRH26 and HRH27. A colony containing the deletion was cured of pRP1099 to yield Δ*efp* *B. anthracis*. The deletion was further confirmed by whole genome sequencing (MiGS SeqCenter).

Complementation of *efp* and *yfmR* in *B. anthracis*

We first constructed a plasmid to integrate genes under the control of an IPTG inducible promoter as a single copy at the *sacA* locus in *B. anthracis*. A DNA fragment (Twist Biosciences) containing 650-bp regions up- and downstream of *sacA* and with 30 bp of homology to pRP1028 at 5' and 3' end was cloned into pRP1028 by Gibson assembly, producing pHRH190. The DNA fragment was designed with a BamHI site in between the two fragments. *B. anthracis efp* was cloned into pDR111 by assembling pDR111 digested with HindIII and SphI and a Twist fragment containing the *efp* coding sequence to make pHRH101. The region between BamHI and EcoRI of pDR111

containing the hyperspank promoter, efp, and LacI were then amplified using primers HRH54 and HRH67 and cloned into pHRH190 by Gibson assembly. *B. subtilis yfmR* was cloned into pDR111 with primers (HRH157 and HRH158) and then the region between BamHI and EcoRI was moved into pHRH190 using the same method as for the *efp* complementation. Triparental mating was used to deliver the resulting plasmids into *B. anthracis* Δ*efp.* The resulting transconjugant was mated with SS1827 and DH5α pRP1099 for homologous recombination to create a complementation strain that was Δ*efp* + *efp* (HRH318). Insertion of *efp* at *sacA* for complementation was PCR-confirmed with primers HRH60 and HRH61. The plasmid pRP1099 harboring SceI endonuclease was cured from the complemented Δ*efp B. anthracis*.

Sporulation

Sporulation was induced in Difco Sporulation Media (DSM) with aeration for 24 hours at 37˚C. Cultures were serially diluted in Tbase with 1 mM $MgSO_4$ and 10 µL was spot plated on LB agar plates before and after heating at 80˚C for 30 min to kill vegetative cells that had not sporulated. Sporulation efficiency was calculated as the percentage of colony forming units before and after heating. For phase contrast microscopy, sporulating cells (grown for 24 hours in DSM with aeration) were immobilized on 1% agarose pads in PBS mounted on microscope slides. Microscopy was performed using a Nikon Eclipse 90i microscope and a CFI Plan Apo 100x, NA 1.45 oil objective.

Macrophage mediated killing assay

B. anthracis wild type (HRH24), Δ*efp,* (HRH126) and Δ*efp* + *efp* (HRH318) were used to infect 10^5 J774A.1 macrophage (Mφ) cells with 10^4 *B. anthracis* wild type, Δ*efp*, or Δ*efp* + *efp* cells to give a multiplicity of infection (MOI) of 0.1:1. IPTG was added to a final concentration of 1 mM to induce *efp* expression in the Δ*efp* + *efp* complementation cultures. The infected macrophages

were incubated in 96-well microplates for 2 hours at 37 °C with 5% CO_2. 100 µL were removed and serially diluted in PBS and plated onto LB agar to enumerate surviving bacterial cells.

Tn-seq library and sequencing

Magellan 6x in vitro transposed gDNA prepared from wild-type *B. subtilis* 168 (52) was transformed into wild type or Δ*efp B. subtilis*. 40 µg of gDNA was transformed into 10 mL of cells made naturally competent (72). Over 400,000 colonies from each library were pooled in 200 mL of LB. gDNA was extracted and sequencing libraries prepared in triplicate from 5 mL each of culture as described previously (52). Briefly, 6 µg gDNA was digested with 3 units of MmeI for 2.5 hours at 37 °C, then treated with 6 units of antarctic phosphatase for 1 hour at 37 °C. DNA was then extracted with 300 µl phenol:chloroform:isoamyl alcohol (25:24:1) and precipitated with 50 µL 3M sodium acetate and 500 µL isopropyl alcohol. Dried pellets were dissolved in 27.5 µL 2 mM Tris-HCl pH 8.5. The DNA was ligated with one volume of 200-µM annealed adapters HRH-Tn1 and HRH-Tn2 in 1 mM tris-Cl pH 8.5. The ligated DNA was purified with the Qiagen PCR purification kit and amplified with the primers HRH-Tn3 and HRH-Tn4. The resulting 136 base pair band was gel extracted and sequenced on the Illumina MiSeq platform (v3 150 bp kit) at the Cornell University Biotechnology Resource Center. Reads were mapped to the *B. subtilis* 168 *trpC2* genome (NCBI, NC_000964) and tallied using Genius Prime (Biomatters). A volcano plot was created with Graphpad Prism using a two-tailed T-test to determine P-value. Raw sequencing reads are available on Gene Expression Omnibus (accession xxxxx).

CRISPRi knockdown

To construct an sgRNA targeting YfmR, we amplified pJMP2 (53) with primer HRHsgRNA-YfmR containing sgRNA sequence 5'-GTTGATTTTCCTGTTCCGT-3' targeting *yfmR* and the reverse primer HRH175. The amplified construct was treated with DpnI for 1 hour at 37 °C to remove the

template plasmid. The PCR product was gel extracted and reassembled by Gibson assembly (70) to create pJMP2-sgRNA^{yfmR}. The reaction was transformed into DH5α and the sequence was confirmed with Sanger sequencing. pJMP1 carrying CRISPRi dCas9 under the control of a xylose-inducible promoter was transformed into wild-type *B. subtilis* and Δ*efp* for integration at *lacA*. pJMP2-P_{veg} – sgRNA^{yfmR} was transformed into the resulting strains for integration at *amyE*. The resulting *B. subtillis* CRISPRi knockdown strains were grown overnight in the absence of xylose and then back diluted to an OD_{600} of 0.05 in LB. The culture was serially diluted and 10 µL of each dilution was spotted onto LB agar or onto LB agar + 5% xylose.

Proline stalling reporter

For *B. anthracis* the reporter plasmid was first generated by liberating SceI endonuclease with EcoRI and SalI from pRP1099 (69) and subsequently removing CFP with inverse PCR using primers HRH73 and HRH74. Next, the fragment $P_{hyperspank}$–MCS–*lacI* of pDR111 was amplified with HRH36 and HRH37 and cloned into the plasmid by Gibson assembly, producing pHRH270. The plasmid was cut with HindIII and SphI, and the fragment containing $P_{hyperspank}$–3xFLAG–RFP–linker–CFP was ordered as a Twist Bioscience gene fragment and cloned in by Giboson assembly to produce pHRH551. The linker region was modified to have either three-polyprolines (5'-CCA CCT CCG-3'), resulting pHRH609, or five-polyproline motifs (5'-CCA CCA CCA CCA CCC-3'), resulting pHRH605. Modified linker regions were purchased as a gene fragment from Twist Biosciences. The resulting reporter plasmids were sequenced with Plasmidsaurus and conjugated into *B. anthracis* strains by tri-parental mating as described above and selected on kanamycin. For *B. subtilis*, the fragment $P_{hyperspank}$–3xFLAG– RFP–linker–CFP was amplified from pHRH609 (for the 3 proline motif), or pHRH605 (for the 5 proline motif) with primers HRH36 and HRH37 and cloned into pDR111 by Gibson assembly. These reporter plasmids were linearized with ScaI and transformed into *B. subtilis* for double crossover at *amyE*.

Western blotting

Overnight cultures of strains carrying the stalling reporter were normalized to an OD_{600} of 0.05 and induced with 1 mM IPTG. The cultures were grown up to OD_{600} 0.6 and 1.2 at 37˚C to measure stalling at mid- and late-log phase. 0.6 OD units of culture were pelleted and resuspended in lysis buffer (10 mM Tris pH 8, 50 mM EDTA, 1 mg/mL lysozyme). After lysis at 37˚C for 10 minutes, 4x SDS loading dye was added to the cell suspension and separated on a 12% SDS-PAGE gel run at 150 V for 70 minutes. Proteins were transferred to PVDF membrane (BioRad) at 300 mAmps for 100 minutes. The membrane was blocked with 3% bovine serum albumin (BSA) for 1 hour at room temperature. 1 µL of anti-FLAG antibody conjugated to Horseradish Peroxidase (Sigma SAB4200119) in 10 mL of PBS-T was incubated overnight at 4˚C. The blot was washed 3 times in TBS-T and developed by using ECL substrate and enhancer (Biorad 170-5060) for detection of full length and truncated bands indicating ribosome stalling. For western blotting against HPF, 10 µL of each fraction collected from a sucrose density gradient was combined with 4X SDS-loading buffer and separated by SDS-PAGE. Protein was transferred to PVDF membrane at 300 mAmps for 90 minutes, blocked with 3% BSA and incubated with a polyclonal antibody raised against *B. subtilis* HPF (59) for 1 hour room temperature. The blot was then washed 3 times in TBS-T and incubated with secondary anti-rabbit antibody conjugated to HRP for 30 minutes at room temperature. The blot was then washed 3 times in TBS-T and developed with ECL (BioRad 170-5060).

Sucrose gradient fractionation

B. subtilis and *B. anthracis* cells were grown overnight at 37 °C and inoculated to an OD_{600} of 0.05 in 50 ml LB. The LB media was supplemented with 1 mM IPTG for the EF-P complementation strain. Log phase culture (~OD 0.6) was collected by centrifugation at 8000 rpm for 10 minutes (Beckman Coulter Avanti J-15R, rotor JA-10.100). The pellets were resuspended in 200 µl gradient buffer containing 20 mM Tris (pH 7.4 at 4˚C), 0.5 mM EDTA, 60 mM NH_4Cl, and 7.5 mM

Mg_2 (55). The cell resuspension was lysed using a homogenizer (Beadbug6, Benchmark) by four 30 s pulses at speed 4350 rpm with chilling on ice for 3 min between the cycles and clarified by ultracentrifugation at 21,300 rcf for 20 min (Eppendorf 5425R, rotor FA-24x2). Clarified cell lysates were normalized to 1500 ng/µl and loaded onto 10 – 40% sucrose gradients in gradient buffer. Ultracentrifugation separated ribosome species at 30,000 rpm for 3 hours at 4°C (Beckman Coulter, rotor SW-41Ti). Gradients were collected using a Biocomp Gradient Station (BioComp Instruments) with A260 continuous readout (Triax full spectrum flow cell). The area under each peak for 30S, 50S, and 70S and the several peaks for polysomes, was quantified using Prism (GraphPad).

Northern blotting and RNA gels

RNA from 0.5 mL of sucrose gradient fractions were precipitated with 1.5 mL of 200 proof ethanol and incubated overnight at -20 °C. The sample pellets were collected by centrifugation at 14,500 rpm for 30 minutes at 4°C (Eppendorf 5425R, rotor FA-24x2). After drying the pellets for 20 minutes at 4°C, pellets were dissolved in 80 µL of nuclease-free water (VWR) and normalized to 1 µg RNA in 5 µL nuclease-free water, mixed with 5 µl 2x RNA loading dye (NEB). To normalize loading for northern blots by rRNA, 1 µg RNA for each sample was heated at 65 °C for 5 minutes and loaded onto 1.5 % TBE agarose supplemented with 3 µL of 10 mg/ml ethidium bromide at 90 V for 1 hour. Bands were quantified and normalized for total rRNA. For detecting fMet-tRNA, RNA normalized as described for each sample was heated at 90 °C for 4 minutes and loaded onto 10 % TBE urea gel (Biorad), then run at 100 V for 110 minutes. The sample RNAs were transferred to Brightstart plus nylon membrane (Invitrogen) at 20 V for 16 hours at 4˚C. The membrane was crosslinked with UV Stratalinker 1800 at 1200 X 100 µJ/cm^2. The crosslinked membrane was pre-hybridized with 20 mL hybridization buffer (Invitrogen) at 45 °C for 1 hour. 10 µL of 20 µM 5' biotinylated tRNA^{fMet} probe (5'-/5Biosg/CGACCTTCGGGTTATGAGCCCGACGAGCTA-3') was added to the pre-hybridized membrane, incubated at 45 °C for 17 hours. The membrane was

washed twice with a buffer containing 1x PBS, and 0.5 % SDS at 45 °C, shaking at 60 rpm. Then washed with a buffer containing 2x sodium saline citrate (SSC, VWR) and 0.5 % SDS at 45 °C, shaking at 60 rpm. The washed membrane was blocked with 20 mL of 3% BSA in 1x PBS + 0.5 % SDS at room temperature for 1 hour. We then added 2 µL 1.25 mg/ml streptavidin-HRP (Thermo Scientific) to the 20 mL blocking solution and incubated for 1 hour. The membrane was then washed with wash buffer (1x PBS and 0.5 % SDS) three times and the blot was developed with 0.8 mL ECL reagent (BioRad) and imaged using a ChemiDoc MP imaging system (BioRad). tRNA sequences for probe design were obtained from GtRNAdb version 2.0 (73, 74). Band intensity for $tRNA^{fMet}$ was compared to band intensity of the 16S rRNA in same sample to determine the ratio of $tRNA^{fMet}$ relative to the amount of small ribosomal subunit.

Structure modeling and sequence comparison of ABCFs

The *E. coli* EttA structure was obtained from Protein Data Bank (PDB 3J5S) (54), YfmR structures for *B. subtilis* and *B. anthracis* were generated with AlphaFold (61). Molecular graphics and analysis were performed with ChimeraX version 1.5 (75). ABCF protein sequences were downloaded from NCBI *E. coli* str. K-12 substr. MG1655 (NC_000913.3) and *B. subtilis* subsp. subtilis str. 168 (NC_000964.3) reference genomes as annotated by the NCBI Prokaryotic Genome Annotation Pipeline (76). Homologs in *B. anthracis* str. Sterne (NZ_CP009541.1) were identified by searching *B. subtilis* ABCF protein sequences (YfmM, YdiF, YfmR, YkpA) against all annotated *B. anthracis* protein sequences using HMMER v3.3 (phmmer) (77). Hits with E-values below 1e-50 and scores above 175 were used for further analyses. ABCF protein sequences were aligned using MAFFT v7.453 (78). The alignment was used to build a phylogenetic tree in RAxML v8.2.12 using the PROTGAMMAAUTO and autoMRE options (79). The tree was midpoint rooted using the phangorn package v2.11.1 (80) and visualized using ggtree v3.6.2 (81).

Acknowledgements

We are grateful to Scott Stibitz and Roger Plaut for sharing pRP1099, pRP1028, pSS1827 and for their generous advice on constructing gene deletions in *B. anthracis* Sterne. We are grateful to Christopher Johnson and Alan Grossman for sharing their transposon library. HAF, HRH and CRP were supported by NIH R35GM147049. LW was supported by an undergraduate research fellowship from the Cornell Institute of Host-Microbe Interactions and Disease.

Table 1

Strain	Description	Source
B. anthracis Sterne	wild-type strain 34F2	
B. anthracis Δ*efp*	in frame unmarked *efp* deletion	This study
B. anthracis Δ*efp sacA::*$P_{hyperspank}$*-efp*	*B. anthracis* Δ*efp* expressing EF-P under IPTG inducible promoter	This study
B. anthracis Δ*efp sacA::*$P_{hyperspank}$*-yfmR*^{Bs}	*B. anthracis* Δ*efp* expressing *B. subtilis* YfmR under IPTG inducible promoter	This study
B. anthracis (pHRH270)	wild-type strain harboring IPTG-inducible pHRH270	This study
B. anthracis (pHRH551)	wild-type strain harboring pHRH270 $P_{hyperspank}$*-3xFLAG-rfp-cfp*	This study
B. anthracis (pHRH605)	wild-type strain harboring pHRH270 $P_{hyperspank}$*-3xFLAG-rfp-5xPro-cfp*	This study
B. anthracis (pHRH609)	wild-type strain harboring pHRH270 $P_{hyperspank}$*-3xFLAG-rfp-3xPro-cfp*	This study
B. anthracis Δ*efp* (pHRH270)	Δ*efp* strain harboring IPTG-inducible pHRH270	This study
B. anthracis Δ*efp* (pHRH551)	Δ*efp* strain harboring pHRH270 $P_{hyperspank}$*-3xFLAG-rfp-cfp*	This study
B. anthracis Δ*efp* (pHRH605)	Δ*efp* strain harboring pHRH270 $P_{hyperspank}$*-3xFLAG-rfp-5xPro-cfp*	This study
B. anthracis Δ*efp* (pHRH609)	Δ*efp* strain harboring pHRH270 $P_{hyperspank}$*-3xFLAG-rfp-3xPro-cfp*	This study
168 *trpC2*	wild-type strain	(82)
168 trpC2 Δ*efp::kan*	*efp* deletion marked with kanamycin resistance	(34)
168 trpC2 Δ*efp*	markerless *efp* deletion	This study
168 trpC2 Δ*yfmR::kan*	*yfmR* deletion marked with kanamycin resistance	This study

Plasmid	Description	Source
pJMP1-dCas9	xylose-inducible CRISPRi dCas9	(53)
pJMP2-sgRNA^{yfmR}	for CRISPRi knockdown to YfmR	This study
pHRH28	for in-frame deletion of *efp* from *B. anthracis*	This study
pHRH101	*B. anthracis efp* cloned into pDR111	This study
pHRH190	*B. anthracis sacA* integrating plasmid	This study
pHRH190 $P_{hyperspank}$–*efp*	*B. anthracis efp* complementation at *sacA*	This study
pHRH190 $P_{hyperspank}$–*yfmR*^{Bs}	*B. subtilis yfmR* complementation at *sacA*	This study
pHRH270	IPTG-inducible plasmid for *B. anthracis*	This study
pHRH551	$P_{hyperspank}$-*3xFLAG-rfp-cfp* cloned into pHRH270	This study
pHRH605	$P_{hyperspank}$-*3xFLAG-rfp-5xPro-cfp* cloned into pHRH270	This study
pHRH609	$P_{hyperspank}$-*3xFLAG-rfp-3xPro-cfp* cloned into pHRH270	This study

Primer	Sequence
HRH-Tn1	5’-gttcagagttctacagtccgacgatcacacNN-3'
HRH-Tn2	5’-gtgtgatcgtcggactgtagaactctgaacgtgta-3'
HRH-Tn3	5’-tcgtcggcagcgtcagatgtgtataagagacagcagagttctacagtccgacgatcacac-3'
HRH-Tn4	5’-gtctcgtgggctcggagatgtgtataagagacagagaccggggacttatcatccaacctg-3'
HRH sgRNA-YfmR	5’- gctcgtgttgtacaataaatgtagttgattttcctgttccgttgttttagagctagaaatagcaagttaaaataaggc-3'

41	HRH175	5’-acatttattgtacaacacgagcc-3'
42	HRH26	5’-atgatttcagtaaacgattttcgtacaggt-3’
43	HRH27	5’-ctatgcacgagaaacgtatttaccttcac-3'
44	HRH36	5’-cctctgttgtccctttctgagaattcgactctagcttgaggcatc-3'
45	HRH37	5’-cttcgttcttttgtcgaggtcgacggatcctaactccattaattgcgttgc-3'
46	HRH54	5’-ttttaagggtaacaattaattcataggatcctaactcacattaattgcgttgc-3'
47	HRH60	5’-tattaactgggagcgtatgcc-3'
48	HRH61	5’-taatagcagcagcaacgttagc-3'
49	HRH67	5’-acttctcttttgaattcaaaaaaaaagactctctagcttgaggcatcaaat-3'
50	HRH73	5’-gtcgacctcgacaaaagaac-3'
51	HRH74	5’-caacaaacatcaaaacaattcatccag-3'
52	HRH157	5’-attgtgagcggataacaattaagcttggaggaaaaaaaatgagcatattaaaagcggaa-3'
53	HRH158	5’-acctcgtttccaccgaattagcttgcatgcttagctttccagttcttcga-3'

References

1. Schmeing TM, Ramakrishnan V. What recent ribosome structures have revealed about the mechanism of translation. Nature. 2009;461(7268):1234-42. Epub 2009/10/20. doi: 10.1038/nature08403. PubMed PMID: 19838167.
2. Guenneugues M, Caserta E, Brandi L, Spurio R, Meunier S, Pon CL, Boelens R, Gualerzi CO. Mapping the fMet-tRNA(f)(Met) binding site of initiation factor IF2. Embo j. 2000;19(19):5233-40. Epub 2000/10/03. doi: 10.1093/emboj/19.19.5233. PubMed PMID: 11013225; PMCID: PMC302095.
3. Simonetti A, Marzi S, Myasnikov AG, Fabbretti A, Yusupov M, Gualerzi CO, Klaholz BP. Structure of the 30S translation initiation complex. Nature. 2008;455(7211):416-20. Epub 2008/09/02. doi: 10.1038/nature07192. PubMed PMID: 18758445.
4. Hussain T, Llácer JL, Wimberly BT, Kieft JS, Ramakrishnan V. Large-Scale Movements of IF3 and tRNA during Bacterial Translation Initiation. Cell. 2016;167(1):133-44.e13. Epub 2016/09/24. doi: 10.1016/j.cell.2016.08.074. PubMed PMID: 27662086; PMCID: PMC5037330.
5. Pape T, Wintermeyer W, Rodnina MV. Complete kinetic mechanism of elongation factor Tu-dependent binding of aminoacyl-tRNA to the A site of the E. coli ribosome. Embo j. 1998;17(24):7490-7. Epub 1998/12/19. doi: 10.1093/emboj/17.24.7490. PubMed PMID: 9857203; PMCID: PMC1171092.
6. Czworkowski J, Moore PB. The elongation phase of protein synthesis. Prog Nucleic Acid Res Mol Biol. 1996;54:293-332. Epub 1996/01/01. doi: 10.1016/s0079-6603(08)60366-9. PubMed PMID: 8768078.
7. Traut RR, Monro RE. The Puromycin reaction and relation to protein synthesis. J Mol Biol. 1964;10:63-72. Epub 1964/10/01. doi: 10.1016/s0022-2836(64)80028-0. PubMed PMID: 14222897.
8. Nissen P, Hansen J, Ban N, Moore PB, Steitz TA. The structural basis of ribosome activity in peptide bond synthesis. Science. 2000;289(5481):920-30. Epub 2000/08/11. doi: 10.1126/science.289.5481.920. PubMed PMID: 10937990.
9. Simonović M, Steitz TA. A structural view on the mechanism of the ribosome-catalyzed peptide bond formation. Biochim Biophys Acta. 2009;1789(9-10):612-23. Epub 2009/07/15. doi: 10.1016/j.bbagrm.2009.06.006. PubMed PMID: 19595805; PMCID: PMC2783306.
10. Rodnina MV, Savelsbergh A, Katunin VI, Wintermeyer W. Hydrolysis of GTP by elongation factor G drives tRNA movement on the ribosome. Nature. 1997;385(6611):37-41. Epub 1997/01/02. doi: 10.1038/385037a0. PubMed PMID: 8985244.
11. Johnson GE, Lalanne JB, Peters ML, Li GW. Functionally uncoupled transcription-translation in Bacillus subtilis. Nature. 2020;585(7823):124-8. Epub 2020/08/28. doi: 10.1038/s41586-020-2638-5. PubMed PMID: 32848247; PMCID: PMC7483943.
12. Lawson MR, Lessen LN, Wang J, Prabhakar A, Corsepius NC, Green R, Puglisi JD. Mechanisms that ensure speed and fidelity in eukaryotic translation termination. Science. 2021;373(6557):876-82. Epub 2021/08/21. doi: 10.1126/science.abi7801. PubMed PMID: 34413231; PMCID: PMC9017434.

13. Wilson DN, Nierhaus KH. The weird and wonderful world of bacterial ribosome regulation. Crit Rev Biochem Mol Biol. 2007;42(3):187-219. Epub 2007/06/15. doi: 10.1080/10409230701360843. PubMed PMID: 17562451.
14. Kyrpides NC, Woese CR. Universally conserved translation initiation factors. Proc Natl Acad Sci U S A. 1998;95(1):224-8. Epub 1998/02/21. doi: 10.1073/pnas.95.1.224. PubMed PMID: 9419357; PMCID: PMC18182.
15. Atkinson GC. The evolutionary and functional diversity of classical and lesser-known cytoplasmic and organellar translational GTPases across the tree of life. BMC Genomics. 2015;16(1):78. Epub 2015/03/11. doi: 10.1186/s12864-015-1289-7. PubMed PMID: 25756599; PMCID: PMC4342817.
16. Starosta AL, Lassak J, Peil L, Atkinson GC, Woolstenhulme CJ, Virumäe K, Buskirk A, Tenson T, Remme J, Jung K, Wilson DN. A conserved proline triplet in Val-tRNA synthetase and the origin of elongation factor P. Cell Rep. 2014;9(2):476-83. Epub 2014/10/15. doi: 10.1016/j.celrep.2014.09.008. PubMed PMID: 25310979; PMCID: PMC4847715.
17. Hummels KR, Kearns DB. Translation elongation factor P (EF-P). FEMS Microbiol Rev. 2020;44(2):208-18. Epub 2020/02/06. doi: 10.1093/femsre/fuaa003. PubMed PMID: 32011712; PMCID: PMC7269679.
18. Schnier J, Schwelberger HG, Smit-McBride Z, Kang HA, Hershey JW. Translation initiation factor 5A and its hypusine modification are essential for cell viability in the yeast Saccharomyces cerevisiae. Mol Cell Biol. 1991;11(6):3105-14. Epub 1991/06/01. doi: 10.1128/mcb.11.6.3105-3114.1991. PubMed PMID: 1903841; PMCID: PMC360154.
19. Patel PH, Costa-Mattioli M, Schulze KL, Bellen HJ. The Drosophila deoxyhypusine hydroxylase homologue nero and its target eIF5A are required for cell growth and the regulation of autophagy. J Cell Biol. 2009;185(7):1181-94. Epub 2009/06/24. doi: 10.1083/jcb.200904161. PubMed PMID: 19546244; PMCID: PMC2712966.
20. Spradling AC, Stern D, Beaton A, Rhem EJ, Laverty T, Mozden N, Misra S, Rubin GM. The Berkeley Drosophila Genome Project gene disruption project: Single P-element insertions mutating 25% of vital Drosophila genes. Genetics. 1999;153(1):135-77. Epub 1999/09/03. doi: 10.1093/genetics/153.1.135. PubMed PMID: 10471706; PMCID: PMC1460730.
21. Kemper WM, Berry KW, Merrick WC. Purification and properties of rabbit reticulocyte protein synthesis initiation factors M2Balpha and M2Bbeta. J Biol Chem. 1976;251(18):5551-7. Epub 1976/09/25. PubMed PMID: 965377.
22. Gutierrez E, Shin BS, Woolstenhulme CJ, Kim JR, Saini P, Buskirk AR, Dever TE. eIF5A promotes translation of polyproline motifs. Mol Cell. 2013;51(1):35-45. Epub 2013/06/04. doi: 10.1016/j.molcel.2013.04.021. PubMed PMID: 23727016; PMCID: PMC3744875.
23. Schuller AP, Wu CC, Dever TE, Buskirk AR, Green R. eIF5A Functions Globally in Translation Elongation and Termination. Mol Cell. 2017;66(2):194-205.e5. Epub 2017/04/11. doi: 10.1016/j.molcel.2017.03.003. PubMed PMID: 28392174; PMCID: PMC5414311.
24. Dever TE, Dinman JD, Green R. Translation Elongation and Recoding in Eukaryotes. Cold Spring Harb Perspect Biol. 2018;10(8). Epub 2018/04/04. doi: 10.1101/cshperspect.a032649. PubMed PMID: 29610120; PMCID: PMC6071482.
25. Guo Q, Cui B, Wang M, Li X, Tan H, Song S, Zhou J, Zhang LH, Deng Y. Elongation factor P modulates Acinetobacter baumannii physiology and virulence as a cyclic dimeric guanosine monophosphate effector. Proc Natl Acad Sci U S A. 2022;119(41):e2209838119. Epub 2022/10/04. doi: 10.1073/pnas.2209838119. PubMed PMID: 36191190; PMCID: PMC9564936.

26. Yanagisawa T, Takahashi H, Suzuki T, Masuda A, Dohmae N, Yokoyama S. Neisseria meningitidis Translation Elongation Factor P and Its Active-Site Arginine Residue Are Essential for Cell Viability. PLoS One. 2016;11(2):e0147907. Epub 2016/02/04. doi: 10.1371/journal.pone.0147907. PubMed PMID: 26840407; PMCID: PMC4739656.
27. DeJesus MA, Gerrick ER, Xu W, Park SW, Long JE, Boutte CC, Rubin EJ, Schnappinger D, Ehrt S, Fortune SM, Sassetti CM, Ioerger TR. Comprehensive Essentiality Analysis of the Mycobacterium tuberculosis Genome via Saturating Transposon Mutagenesis. mBio. 2017;8(1). Epub 2017/01/18. doi: 10.1128/mBio.02133-16. PubMed PMID: 28096490; PMCID: PMC5241402.
28. Tollerson R, 2nd, Witzky A, Ibba M. Elongation factor P is required to maintain proteome homeostasis at high growth rate. Proc Natl Acad Sci U S A. 2018;115(43):11072-7. Epub 2018/10/10. doi: 10.1073/pnas.1812025115. PubMed PMID: 30297417; PMCID: PMC6205485.
29. Hersch SJ, Wang M, Zou SB, Moon KM, Foster LJ, Ibba M, Navarre WW. Divergent protein motifs direct elongation factor P-mediated translational regulation in Salmonella enterica and Escherichia coli. mBio. 2013;4(2):e00180-13. Epub 2013/04/25. doi: 10.1128/mBio.00180-13. PubMed PMID: 23611909; PMCID: PMC3638311.
30. Balibar CJ, Iwanowicz D, Dean CR. Elongation factor P is dispensable in Escherichia coli and Pseudomonas aeruginosa. Curr Microbiol. 2013;67(3):293-9. Epub 2013/04/18. doi: 10.1007/s00284-013-0363-0. PubMed PMID: 23591475.
31. Rajkovic A, Hummels KR, Witzky A, Erickson S, Gafken PR, Whitelegge JP, Faull KF, Kearns DB, Ibba M. Translation Control of Swarming Proficiency in Bacillus subtilis by 5-Amino-pentanolylated Elongation Factor P. J Biol Chem. 2016;291(21):10976-85. Epub 2016/03/24. doi: 10.1074/jbc.M115.712091. PubMed PMID: 27002156; PMCID: PMC4900249.
32. Witzky A, Hummels KR, Tollerson R, 2nd, Rajkovic A, Jones LA, Kearns DB, Ibba M. EF-P Posttranslational Modification Has Variable Impact on Polyproline Translation in Bacillus subtilis. mBio. 2018;9(2). Epub 2018/04/05. doi: 10.1128/mBio.00306-18. PubMed PMID: 29615499; PMCID: PMC5885033.
33. Hummels KR, Kearns DB. Suppressor mutations in ribosomal proteins and FliY restore Bacillus subtilis swarming motility in the absence of EF-P. PLoS Genet. 2019;15(6):e1008179. Epub 2019/06/27. doi: 10.1371/journal.pgen.1008179. PubMed PMID: 31237868; PMCID: PMC6613710.
34. Feaga HA, Hong HR, Prince CR, Rankin A, Buskirk AR, Dworkin J. Elongation Factor P Is Important for Sporulation Initiation. J Bacteriol. 2023;205(2):e0037022. Epub 2023/01/19. doi: 10.1128/jb.00370-22. PubMed PMID: 36651772; PMCID: PMC9945569.
35. Glick BR, Chládek S, Ganoza MC. Peptide bond formation stimulated by protein synthesis factor EF-P depends on the aminoacyl moiety of the acceptor. Eur J Biochem. 1979;97(1):23-8. Epub 1979/06/01. doi: 10.1111/j.1432-1033.1979.tb13081.x. PubMed PMID: 383483.
36. Doerfel LK, Wohlgemuth I, Kothe C, Peske F, Urlaub H, Rodnina MV. EF-P is essential for rapid synthesis of proteins containing consecutive proline residues. Science. 2013;339(6115):85-8. Epub 2012/12/15. doi: 10.1126/science.1229017. PubMed PMID: 23239624.
37. Peil L, Starosta AL, Lassak J, Atkinson GC, Virumae K, Spitzer M, Tenson T, Jung K, Remme J, Wilson DN. Distinct XPPX sequence motifs induce ribosome stalling, which is rescued by the translation elongation factor EF-P. Proc Natl Acad Sci U S A. 2013;110(38):15265-70.

Epub 2013/09/05. doi: 10.1073/pnas.1310642110. PubMed PMID: 24003132; PMCID: PMC3780873.
38. Ude S, Lassak J, Starosta AL, Kraxenberger T, Wilson DN, Jung K. Translation elongation factor EF-P alleviates ribosome stalling at polyproline stretches. Science. 2013;339(6115):82-5. Epub 2012/12/15. doi: 10.1126/science.1228985. PubMed PMID: 23239623.
39. Bullwinkle TJ, Zou SB, Rajkovic A, Hersch SJ, Elgamal S, Robinson N, Smil D, Bolshan Y, Navarre WW, Ibba M. (R)-β-lysine-modified elongation factor P functions in translation elongation. J Biol Chem. 2013;288(6):4416-23. Epub 2013/01/02. doi: 10.1074/jbc.M112.438879. PubMed PMID: 23277358; PMCID: PMC3567691.
40. Doerfel LK, Wohlgemuth I, Kubyshkin V, Starosta AL, Wilson DN, Budisa N, Rodnina MV. Entropic Contribution of Elongation Factor P to Proline Positioning at the Catalytic Center of the Ribosome. J Am Chem Soc. 2015;137(40):12997-3006. Epub 2015/09/19. doi: 10.1021/jacs.5b07427. PubMed PMID: 26384033.
41. Gamper HB, Masuda I, Frenkel-Morgenstern M, Hou YM. Maintenance of protein synthesis reading frame by EF-P and m(1)G37-tRNA. Nat Commun. 2015;6:7226. Epub 2015/05/27. doi: 10.1038/ncomms8226. PubMed PMID: 26009254; PMCID: PMC4445466.
42. Chevance FF, Le Guyon S, Hughes KT. The effects of codon context on in vivo translation speed. PLoS Genet. 2014;10(6):e1004392. Epub 2014/06/06. doi: 10.1371/journal.pgen.1004392. PubMed PMID: 24901308; PMCID: PMC4046918.
43. Johansson M, Ieong KW, Trobro S, Strazewski P, Åqvist J, Pavlov MY, Ehrenberg M. pH-sensitivity of the ribosomal peptidyl transfer reaction dependent on the identity of the A-site aminoacyl-tRNA. Proc Natl Acad Sci U S A. 2011;108(1):79-84. Epub 2010/12/21. doi: 10.1073/pnas.1012612107. PubMed PMID: 21169502; PMCID: PMC3017169.
44. Muto H, Ito K. Peptidyl-prolyl-tRNA at the ribosomal P-site reacts poorly with puromycin. Biochem Biophys Res Commun. 2008;366(4):1043-7. Epub 2007/12/25. doi: 10.1016/j.bbrc.2007.12.072. PubMed PMID: 18155161.
45. Pavlov MY, Watts RE, Tan Z, Cornish VW, Ehrenberg M, Forster AC. Slow peptide bond formation by proline and other N-alkylamino acids in translation. Proc Natl Acad Sci U S A. 2009;106(1):50-4. Epub 2008/12/24. doi: 10.1073/pnas.0809211106. PubMed PMID: 19104062; PMCID: PMC2629218.
46. Wohlgemuth I, Brenner S, Beringer M, Rodnina MV. Modulation of the rate of peptidyl transfer on the ribosome by the nature of substrates. J Biol Chem. 2008;283(47):32229-35. Epub 2008/09/24. doi: 10.1074/jbc.M805316200. PubMed PMID: 18809677.
47. Yaron A, Naider F. Proline-dependent structural and biological properties of peptides and proteins. Crit Rev Biochem Mol Biol. 1993;28(1):31-81. Epub 1993/01/01. doi: 10.3109/10409239309082572. PubMed PMID: 8444042.
48. Woolstenhulme CJ, Guydosh NR, Green R, Buskirk AR. High-precision analysis of translational pausing by ribosome profiling in bacteria lacking EFP. Cell Rep. 2015;11(1):13-21. Epub 2015/04/07. doi: 10.1016/j.celrep.2015.03.014. PubMed PMID: 25843707; PMCID: PMC4835038.
49. Ranquet C, Gottesman S. Translational regulation of the Escherichia coli stress factor RpoS: a role for SsrA and Lon. J Bacteriol. 2007;189(13):4872-9. Epub 2007/04/24. doi: 10.1128/jb.01838-06. PubMed PMID: 17449615; PMCID: PMC1913435.

50. Shin JH, Price CW. The SsrA-SmpB ribosome rescue system is important for growth of Bacillus subtilis at low and high temperatures. J Bacteriol. 2007;189(10):3729-37. Epub 2007/03/21. doi: 10.1128/jb.00062-07. PubMed PMID: 17369301; PMCID: PMC1913333.
51. Han NC, Kelly P, Ibba M. Translational quality control and reprogramming during stress adaptation. Exp Cell Res. 2020;394(2):112161. Epub 2020/07/04. doi: 10.1016/j.yexcr.2020.112161. PubMed PMID: 32619498.
52. Johnson CM, Grossman AD. Identification of host genes that affect acquisition of an integrative and conjugative element in Bacillus subtilis. Mol Microbiol. 2014;93(6):1284-301. Epub 2014/07/30. doi: 10.1111/mmi.12736. PubMed PMID: 25069588; PMCID: PMC4160349.
53. Peters JM, Colavin A, Shi H, Czarny TL, Larson MH, Wong S, Hawkins JS, Lu CHS, Koo BM, Marta E, Shiver AL, Whitehead EH, Weissman JS, Brown ED, Qi LS, Huang KC, Gross CA. A Comprehensive, CRISPR-based Functional Analysis of Essential Genes in Bacteria. Cell. 2016;165(6):1493-506. Epub 2016/05/31. doi: 10.1016/j.cell.2016.05.003. PubMed PMID: 27238023; PMCID: PMC4894308.
54. Chen B, Boël G, Hashem Y, Ning W, Fei J, Wang C, Gonzalez RL, Jr., Hunt JF, Frank J. EttA regulates translation by binding the ribosomal E site and restricting ribosome-tRNA dynamics. Nat Struct Mol Biol. 2014;21(2):152-9. Epub 2014/01/07. doi: 10.1038/nsmb.2741. PubMed PMID: 24389465; PMCID: PMC4143144.
55. Singh S, Gentry RC, Fu Z, Bailey NA, Altomare CG, Wong K-H, Neky MJ, Wang C, Ray KK, Chi Y-C, Zhang Z, Grassucci RA, Frank J, Boël G, Ruben L. Gonzalez J, Hunt JF. Cryo-EM studies of the four E. coli paralogs establish ABCF proteins as master plumbers of the peptidyl-transferase center of the ribosome. bioRxiv. 2023:2023.06.15.543498. doi: 10.1101/2023.06.15.543498.
56. Smith AM, Costello MS, Kettring AH, Wingo RJ, Moore SD. Ribosome collisions alter frameshifting at translational reprogramming motifs in bacterial mRNAs. Proc Natl Acad Sci U S A. 2019;116(43):21769-79. Epub 2019/10/09. doi: 10.1073/pnas.1910613116. PubMed PMID: 31591196; PMCID: PMC6815119.
57. Basu A, Shields KE, Eickhoff CS, Hoft DF, Yap MN. Thermal and Nutritional Regulation of Ribosome Hibernation in Staphylococcus aureus. J Bacteriol. 2018;200(24). Epub 2018/10/10. doi: 10.1128/jb.00426-18. PubMed PMID: 30297357; PMCID: PMC6256015.
58. Basu A, Shields KE, Yap MF. The hibernating 100S complex is a target of ribosome-recycling factor and elongation factor G in Staphylococcus aureus. J Biol Chem. 2020;295(18):6053-63. Epub 2020/03/27. doi: 10.1074/jbc.RA119.012307. PubMed PMID: 32209660; PMCID: PMC7196661.
59. Feaga HA, Kopylov M, Kim JK, Jovanovic M, Dworkin J. Ribosome Dimerization Protects the Small Subunit. J Bacteriol. 2020;202(10). Epub 2020/03/04. doi: 10.1128/jb.00009-20. PubMed PMID: 32123037; PMCID: PMC7186458.
60. Ousalem F, Singh S, Bailey NA, Wong K-H, Zhu L, Neky MJ, Sibindi C, Fei J, Ruben L. Gonzalez J, Boël G, Hunt JF. Comparative genetic, biochemical, and biophysical analyses of the four E. coli ABCF paralogs support distinct functions related to mRNA translation. bioRxiv. 2023:2023.06.11.543863. doi: 10.1101/2023.06.11.543863.
61. Jumper J, Evans R, Pritzel A, Green T, Figurnov M, Ronneberger O, Tunyasuvunakool K, Bates R, Žídek A, Potapenko A, Bridgland A, Meyer C, Kohl SAA, Ballard AJ, Cowie A, Romera-Paredes B, Nikolov S, Jain R, Adler J, Back T, Petersen S, Reiman D, Clancy E, Zielinski M, Steinegger M, Pacholska M, Berghammer T, Bodenstein S, Silver D, Vinyals O, Senior AW, Kavukcuoglu K, Kohli P, Hassabis D. Highly accurate protein structure prediction with AlphaFold.

Nature. 2021;596(7873):583-9. Epub 2021/07/16. doi: 10.1038/s41586-021-03819-2. PubMed PMID: 34265844; PMCID: PMC8371605 have filed non-provisional patent applications 16/701,070 and PCT/EP2020/084238, and provisional patent applications 63/107,362, 63/118,917, 63/118,918, 63/118,921 and 63/118,919, each in the name of DeepMind Technologies Limited, each pending, relating to machine learning for predicting protein structures. The other authors declare no competing interests.

62. Boël G, Smith PC, Ning W, Englander MT, Chen B, Hashem Y, Testa AJ, Fischer JJ, Wieden HJ, Frank J, Gonzalez RL, Jr., Hunt JF. The ABC-F protein EttA gates ribosome entry into the translation elongation cycle. Nat Struct Mol Biol. 2014;21(2):143-51. Epub 2014/01/07. doi: 10.1038/nsmb.2740. PubMed PMID: 24389466; PMCID: PMC4101993.

63. Nagao A, Nakanishi Y, Yamaguchi Y, Mishina Y, Karoji M, Toya T, Fujita T, Iwasaki S, Miyauchi K, Sakaguchi Y, Suzuki T. Quality control of protein synthesis in the early elongation stage. Nat Commun. 2023;14(1):2704. Epub 2023/05/18. doi: 10.1038/s41467-023-38077-5. PubMed PMID: 37198183; PMCID: PMC10192219.

64. Murina V, Kasari M, Takada H, Hinnu M, Saha CK, Grimshaw JW, Seki T, Reith M, Putrinš M, Tenson T, Strahl H, Hauryliuk V, Atkinson GC. ABCF ATPases Involved in Protein Synthesis, Ribosome Assembly and Antibiotic Resistance: Structural and Functional Diversification across the Tree of Life. J Mol Biol. 2019;431(18):3568-90. Epub 2019/01/01. doi: 10.1016/j.jmb.2018.12.013. PubMed PMID: 30597160; PMCID: PMC6723617.

65. Hoffer ED, Hong S, Sunita S, Maehigashi T, Gonzalez RLJ, Whitford PC, Dunham CM. Structural insights into mRNA reading frame regulation by tRNA modification and slippery codon-anticodon pairing. Elife. 2020;9. Epub 2020/10/06. doi: 10.7554/eLife.51898. PubMed PMID: 33016876; PMCID: PMC7577736.

66. Mohapatra S, Choi H, Ge X, Sanyal S, Weisshaar JC. Spatial Distribution and Ribosome-Binding Dynamics of EF-P in Live Escherichia coli. mBio. 2017;8(3). Epub 2017/06/08. doi: 10.1128/mBio.00300-17. PubMed PMID: 28588135; PMCID: PMC5461404.

67. Hilbert DW, Piggot PJ. Compartmentalization of gene expression during Bacillus subtilis spore formation. Microbiol Mol Biol Rev. 2004;68(2):234-62. Epub 2004/06/10. doi: 10.1128/mmbr.68.2.234-262.2004. PubMed PMID: 15187183; PMCID: PMC419919.

68. Pinheiro B, Petrov DP, Guo L, Martins GB, Bramkamp M, Jung K. Elongation factor P is required for EII(Glc) translation in Corynebacterium glutamicum due to an essential polyproline motif. Mol Microbiol. 2021;115(2):320-31. Epub 2020/10/05. doi: 10.1111/mmi.14618. PubMed PMID: 33012080.

69. Plaut RD, Stibitz S. Improvements to a Markerless Allelic Exchange System for Bacillus anthracis. PLoS One. 2015;10(12):e0142758. Epub 2015/12/02. doi: 10.1371/journal.pone.0142758. PubMed PMID: 26624016; PMCID: PMC4666636.

70. Gibson DG, Young L, Chuang RY, Venter JC, Hutchison CA, 3rd, Smith HO. Enzymatic assembly of DNA molecules up to several hundred kilobases. Nat Methods. 2009;6(5):343-5. Epub 2009/04/14. doi: 10.1038/nmeth.1318. PubMed PMID: 19363495.

71. Stibitz S, Aaronson W, Monack D, Falkow S. The vir locus and phase-variation in Bordetella pertussis. Tokai J Exp Clin Med. 1988;13 Suppl:223-6. Epub 1988/01/01. PubMed PMID: 2908523.

72. Dubnau D, Davidoff-Abelson R. Fate of transforming DNA following uptake by competent Bacillus subtilis. I. Formation and properties of the donor-recipient complex. J Mol

Biol. 1971;56(2):209-21. Epub 1971/03/14. doi: 10.1016/0022-2836(71)90460-8. PubMed PMID: 4994568.
73. Chan PP, Lowe TM. GtRNAdb 2.0: an expanded database of transfer RNA genes identified in complete and draft genomes. Nucleic Acids Res. 2016;44(D1):D184-9. Epub 2015/12/18. doi: 10.1093/nar/gkv1309. PubMed PMID: 26673694; PMCID: PMC4702915.
74. Chan PP, Lowe TM. GtRNAdb: a database of transfer RNA genes detected in genomic sequence. Nucleic Acids Res. 2009;37(Database issue):D93-7. Epub 2008/11/06. doi: 10.1093/nar/gkn787. PubMed PMID: 18984615; PMCID: PMC2686519.
75. Pettersen EF, Goddard TD, Huang CC, Meng EC, Couch GS, Croll TI, Morris JH, Ferrin TE. UCSF ChimeraX: Structure visualization for researchers, educators, and developers. Protein Sci. 2021;30(1):70-82. Epub 2020/09/04. doi: 10.1002/pro.3943. PubMed PMID: 32881101; PMCID: PMC7737788.
76. Li W, O'Neill KR, Haft DH, DiCuccio M, Chetvernin V, Badretdin A, Coulouris G, Chitsaz F, Derbyshire MK, Durkin AS, Gonzales NR, Gwadz M, Lanczycki CJ, Song JS, Thanki N, Wang J, Yamashita RA, Yang M, Zheng C, Marchler-Bauer A, Thibaud-Nissen F. RefSeq: expanding the Prokaryotic Genome Annotation Pipeline reach with protein family model curation. Nucleic Acids Res. 2021;49(D1):D1020-d8. Epub 2020/12/04. doi: 10.1093/nar/gkaa1105. PubMed PMID: 33270901; PMCID: PMC7779008.
77. Eddy SR. Accelerated Profile HMM Searches. PLoS Comput Biol. 2011;7(10):e1002195. Epub 2011/11/01. doi: 10.1371/journal.pcbi.1002195. PubMed PMID: 22039361; PMCID: PMC3197634.
78. Katoh K, Standley DM. MAFFT multiple sequence alignment software version 7: improvements in performance and usability. Mol Biol Evol. 2013;30(4):772-80. Epub 2013/01/19. doi: 10.1093/molbev/mst010. PubMed PMID: 23329690; PMCID: PMC3603318.
79. Stamatakis A. RAxML version 8: a tool for phylogenetic analysis and post-analysis of large phylogenies. Bioinformatics. 2014;30(9):1312-3. Epub 2014/01/24. doi: 10.1093/bioinformatics/btu033. PubMed PMID: 24451623; PMCID: PMC3998144.
80. Schliep KP. phangorn: phylogenetic analysis in R. Bioinformatics. 2011;27(4):592-3. Epub 2010/12/21. doi: 10.1093/bioinformatics/btq706. PubMed PMID: 21169378; PMCID: PMC3035803.
81. Yu G. Using ggtree to Visualize Data on Tree-Like Structures. Curr Protoc Bioinformatics. 2020;69(1):e96. Epub 2020/03/13. doi: 10.1002/cpbi.96. PubMed PMID: 32162851.
82. Gaidenko TA, Kim TJ, Price CW. The PrpC serine-threonine phosphatase and PrkC kinase have opposing physiological roles in stationary-phase Bacillus subtilis cells. J Bacteriol. 2002;184(22):6109-14. Epub 2002/10/26. doi: 10.1128/jb.184.22.6109-6114.2002. PubMed PMID: 12399479; PMCID: PMC151969.

Figure 1

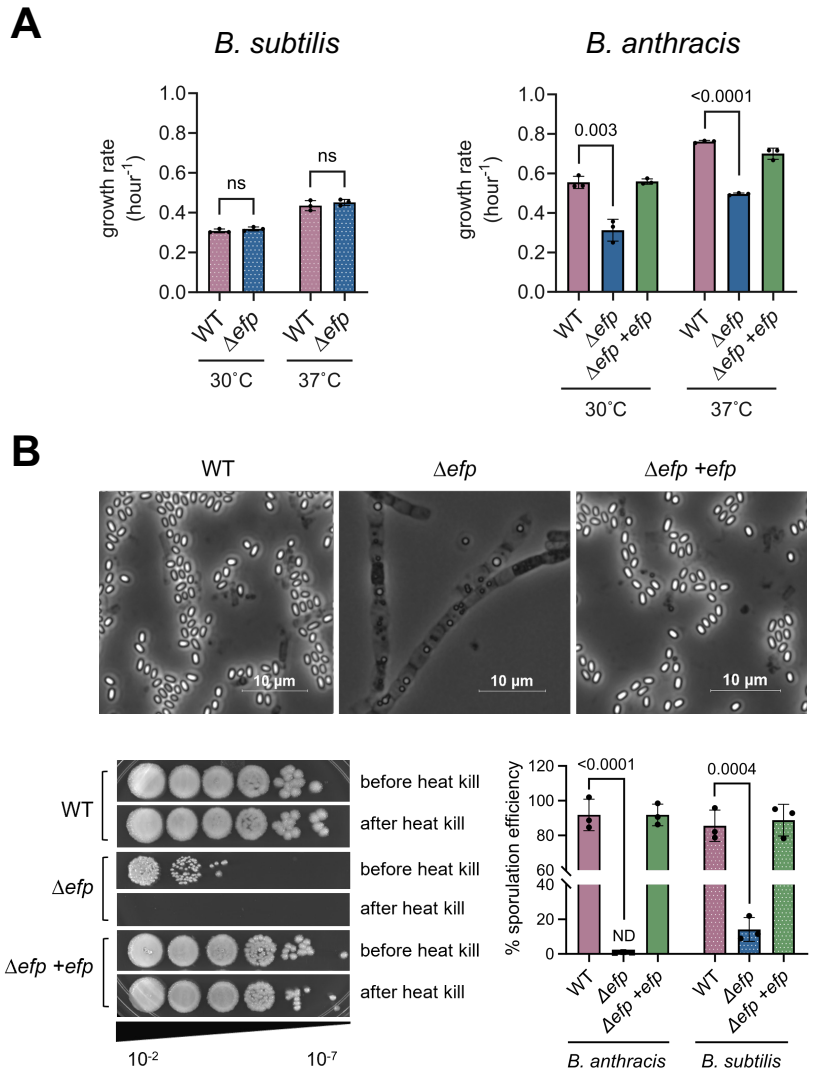

Fig. 1 *Bacillus anthracis* Δ*efp* exhibits severe growth and sporulation defects. (A) *B. subtilis* Δ*efp* exhibits no growth defect in LB at 30˚C or 37˚C. In contrast, *B. anthracis* Δ*efp* exhibits a severe growth defect at both temperatures. (B) *B. anthracis* Δ*efp* does not produce detectable spores. Phase contrast microscopy images of wild type and *B. anthracis* Δ*efp* after 24 hours of sporulation in DSM at 37˚C. Spores appear phase-bright. Δ*efp* cells produce immature spore-forms that do not survive heat killing at 80˚C. *B. anthracis* Δ*efp* also exhibits decreased survival after 24 hours of growth in DSM as measured by enumerating colony forming units. Sporulation efficiency was determined by measuring CFU before and after 30 minutes at 80˚C to kill all non-sporulated cells. Wild-type *B. anthracis* sporulated with >80% efficiency whereas Δ*efp* did not produce detectable spores. The Δ*efp* growth and sporulation defects were complemented with a single copy of *efp* integrated at *sacA*. Error bars represent the standard deviation of 3 biological replicates.

Figure 2

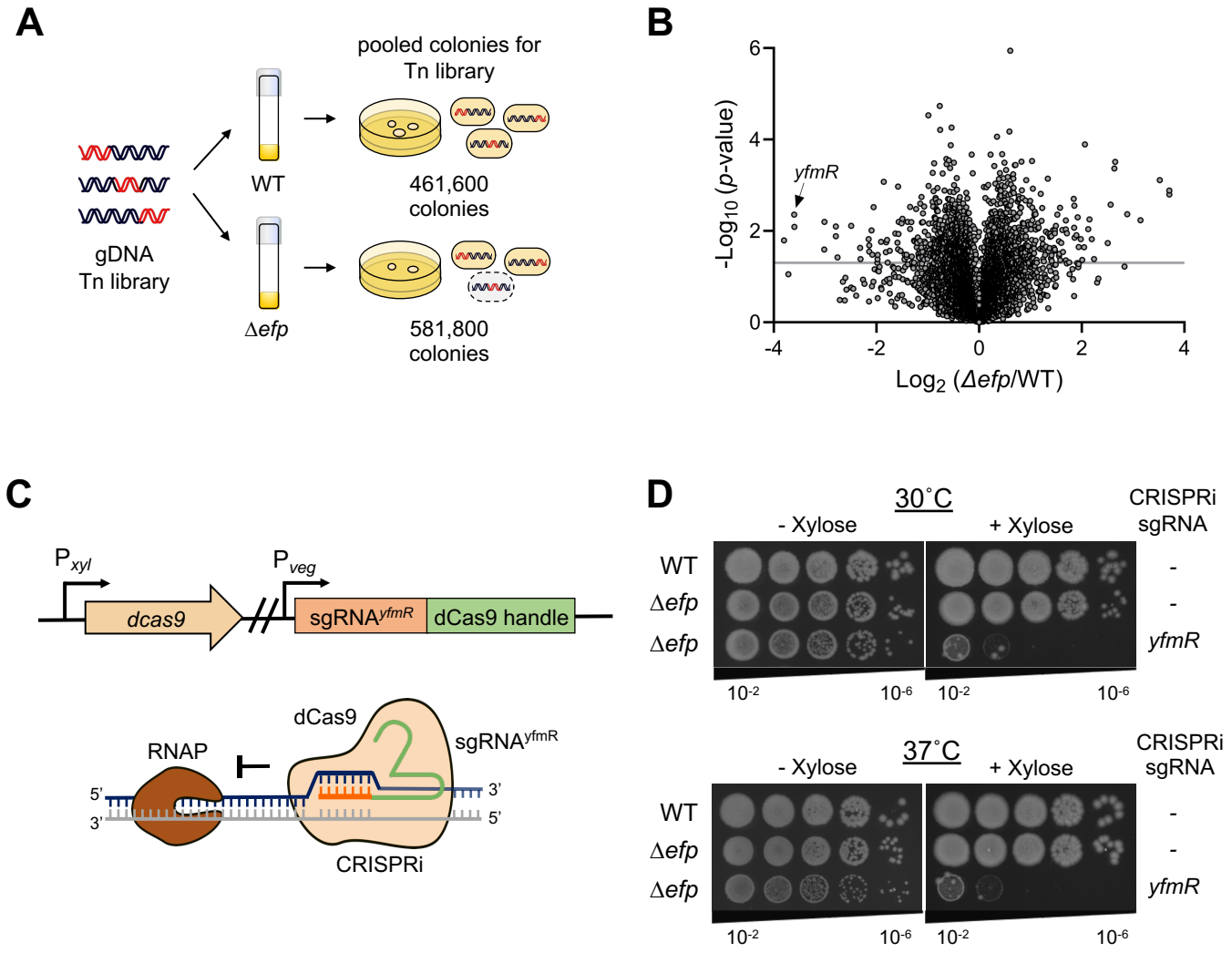

Fig 2. YfmR depletion is lethal to *B. subtilis* Δ*efp*. (A) Schematic of Tn-seq library generation. *In vitro* transposed gDNA was transformed into wild type and Δ*efp B. subtilis*. Transposants were selected on kanamycin and >450,000 colonies were pooled for each strain. Illumina libraries were constructed in triplicate and insertion sites were mapped to the *B. subtilis* 168 chromosome. (B) Volcano plot showing the results of Tn-seq experiment. (C) Schematic of CRISPR interference to deplete YfmR. Guide RNA targeting *yfmR* (sgRNA^{yfmR}) is constitutively expressed while deactivated Cas9 (dCas9) is expressed under the control of a xylose promoter. (D) *B. subtilis* Δ*efp* expressing dCas9+sgRNA^{yfmR} fails to form colonies at 30˚C and 37˚C. Log-phase cultures were serially diluted and then plated with and without xylose for induction of dCas9. Wild type and Δ*efp* strains express dCas9 only, without guide RNA, where indicated. Spot plates are representative of 3 independent experiments.

Figure 3

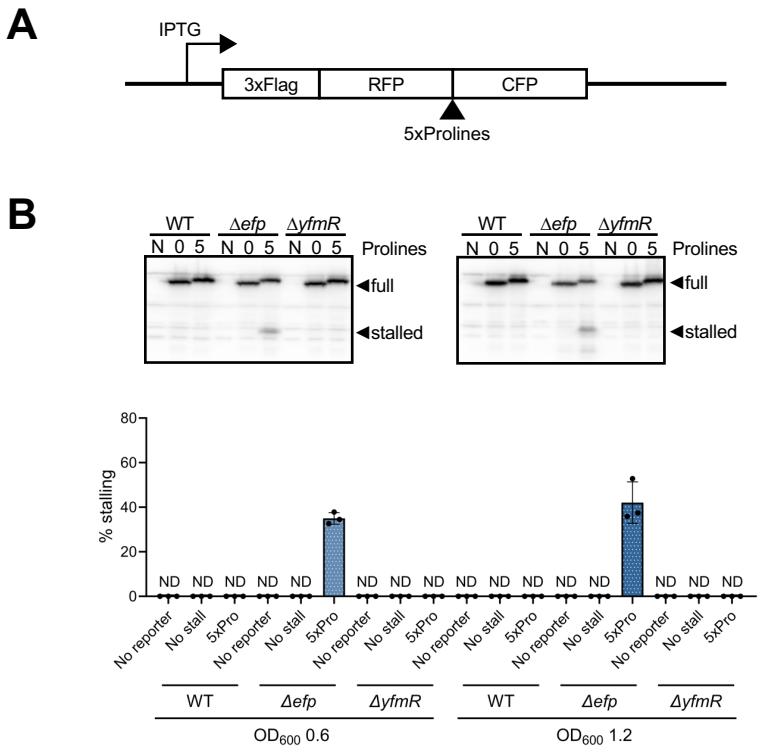

Fig 3. *B. subtilis* Δ*yfmR* does not exhibit increased stalling at a polyproline tract. (A) Stalling reporter encoding a 3xFlag tag-RFP-CFP fusion under the control of an IPTG promoter. 5x prolines (CCA CCA CCA CCA CCC) were inserted between the end of RFP and the start of CFP. (B) Western blot showing full length (full) or truncated peptides (stalled). Truncated peptide indicates a stall at the 5x polyproline motif. (C) Percent stalling was calculated as a ratio of the stalled band intensity to the total band intensity of each strain. N: control strain of the respective background (wild type, Δ*efp*, Δ*yfmR*) without the stalling reporter; 0: control strains harboring reporter without polyproline motif; 5: strains harboring stalling reporter with 5x proline motifs between RFP and CFP. Error bars represent standard deviation of 3 biological replicates. ND indicates not detectable.

Figure 4

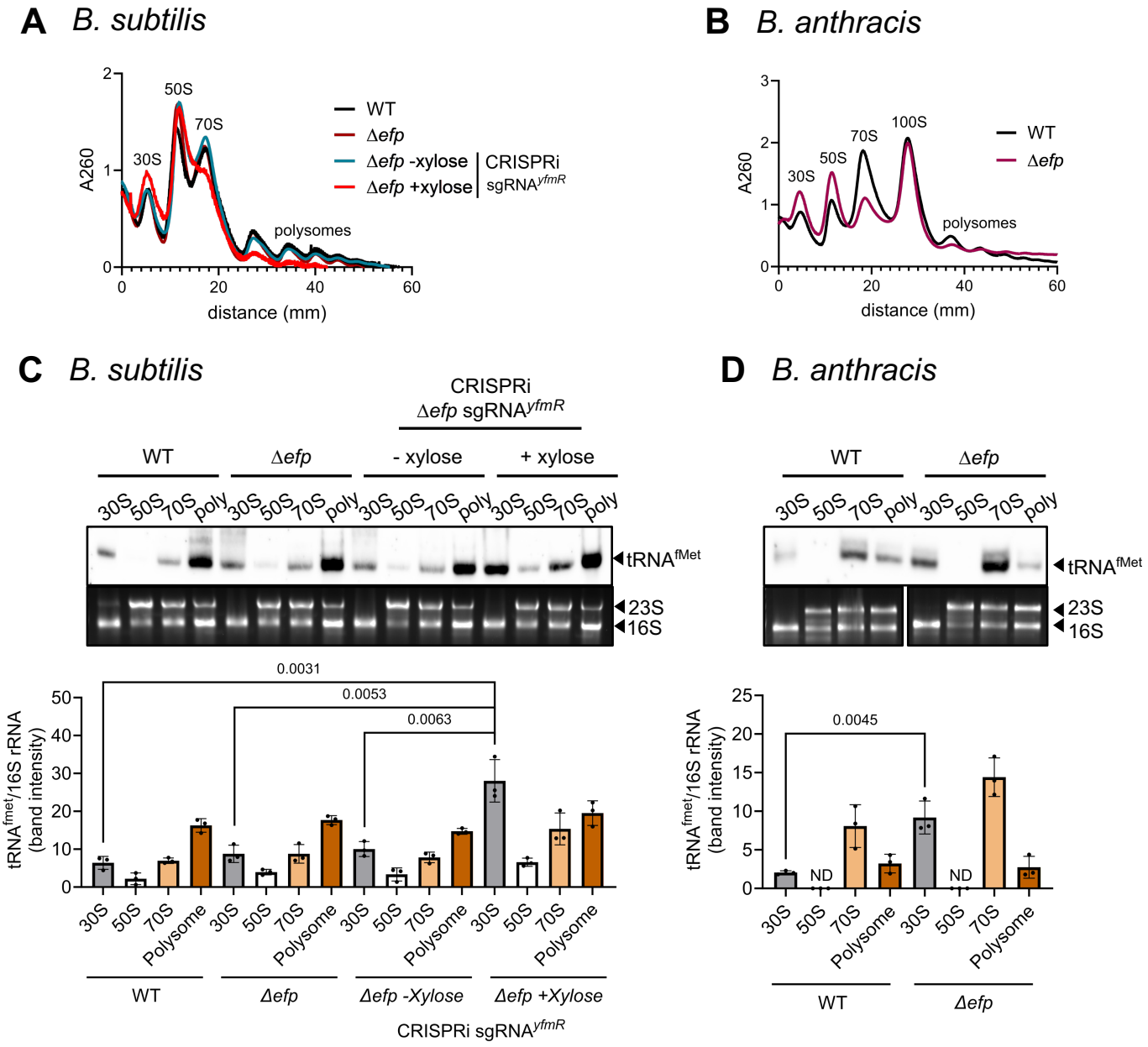

Fig 4. YfmR and EF-P assist translation during early elongation. (A) Representative sucrose density gradient profile showing increased 30S and 50S subunits and decreased 70S ribosomes and polysomes when *yfmR* is depleted in Δ*efp B. subtilis.* Quantification of subunits for 3 biological replicates is shown in Figure S3. (B) The sucrose density gradient profile of *B. anthracis* ribosomes shows increased 30S and 50S subunits and decreased 70S ribosomes and polysomes in Δ*efp* compared to wild type. (C) 30S, 50S, 70S, and polysome fractions were collected and RNA was precipitated, normalized, and resolved on a TBE-urea gel. Levels of $tRNA^{fMet}$ associated with each ribosomal species (30S, 50S, 70S and polysomes) was determined by northern blot. $tRNA^{fMet}$ associated with the 30S small subunit increased when YfmR was depleted in Δ*efp B. subtilis* compared to wild type and Δ*efp* single deletion. (D) Initiator $tRNA^{fMet}$ associated with the 30S small ribosomal subunit increased in Δ*efp B. anthracis* compared to wild type. (Bottom) The ratio of $tRNA^{fMet}$ band intensity to 16S rRNA band intensity for each sample is plotted with error bars representing the standard deviation of 3 biological replicates. P-values are shown above brackets as determined by an unpaired two-tailed T-test.

Figure 5

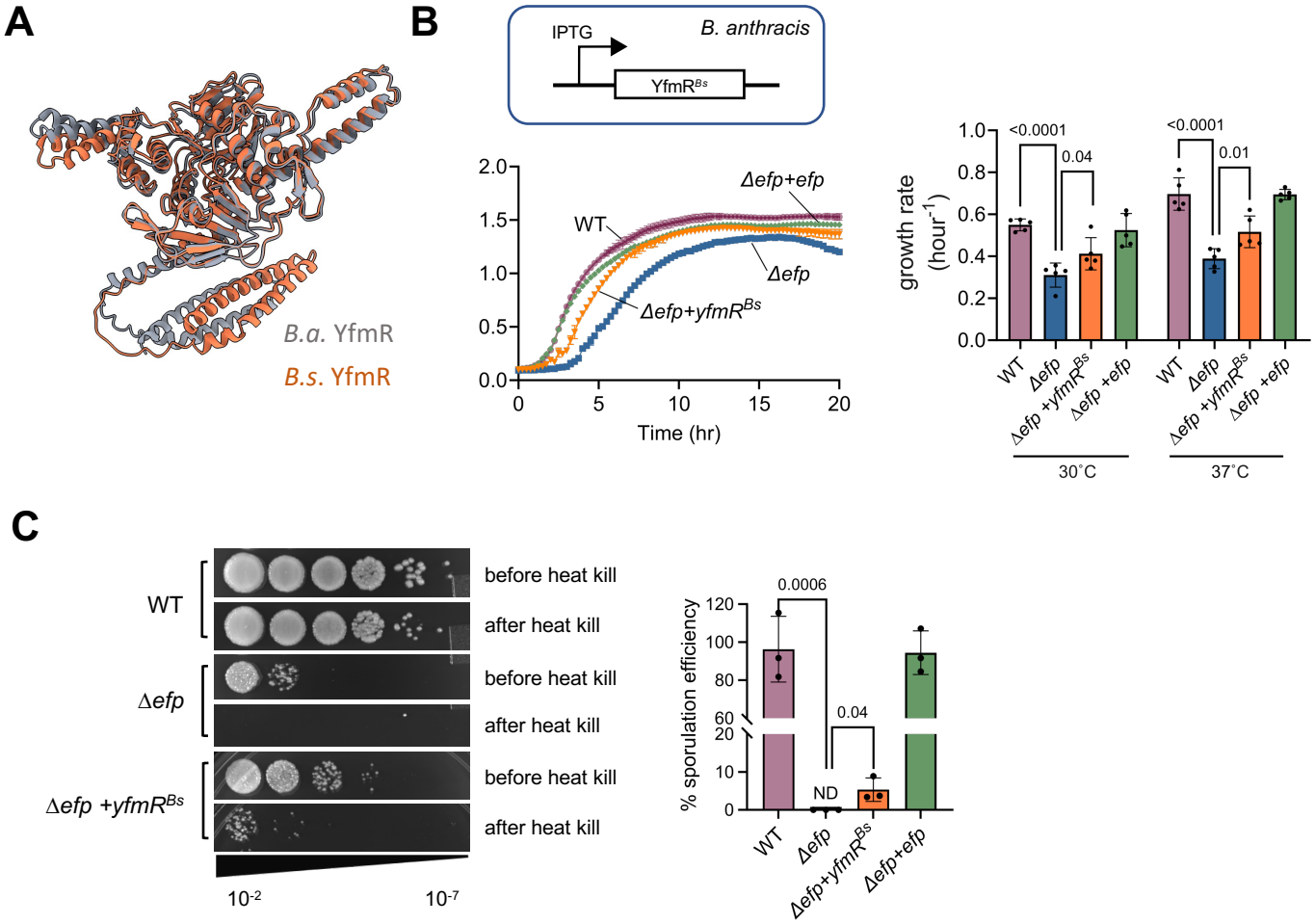

Fig 5. Heterologous expression of *B. subtilis* YfmR in *B. anthracis* Δ*efp* partially rescues growth and sporulation defects. (A) Overlay of predicted YfmR structures from *B. anthracis* and *B. subtilis* generated by AlphaFold. (B) A single copy of *yfmR* from *B. subtilis* (*yfmR*^{Bs}) integrated into the *B. anthracis* chromosome under the control of an IPTG-inducible promoter partially rescues the *B. anthracis* Δ*efp* growth defect. (C) The same construct as in (B) partially rescues the *B. anthracis* Δ*efp* sporulation defect. P-values are shown above brackets and were determined by an unpaired two-tailed T-test. Error bars represent standard deviation of 3 biological replicates for sporulation assay. Growth rate was determined at early log-phase. Error bars on growth rate bar graph represent standard deviation of 5 biological replicates.

Figure 6

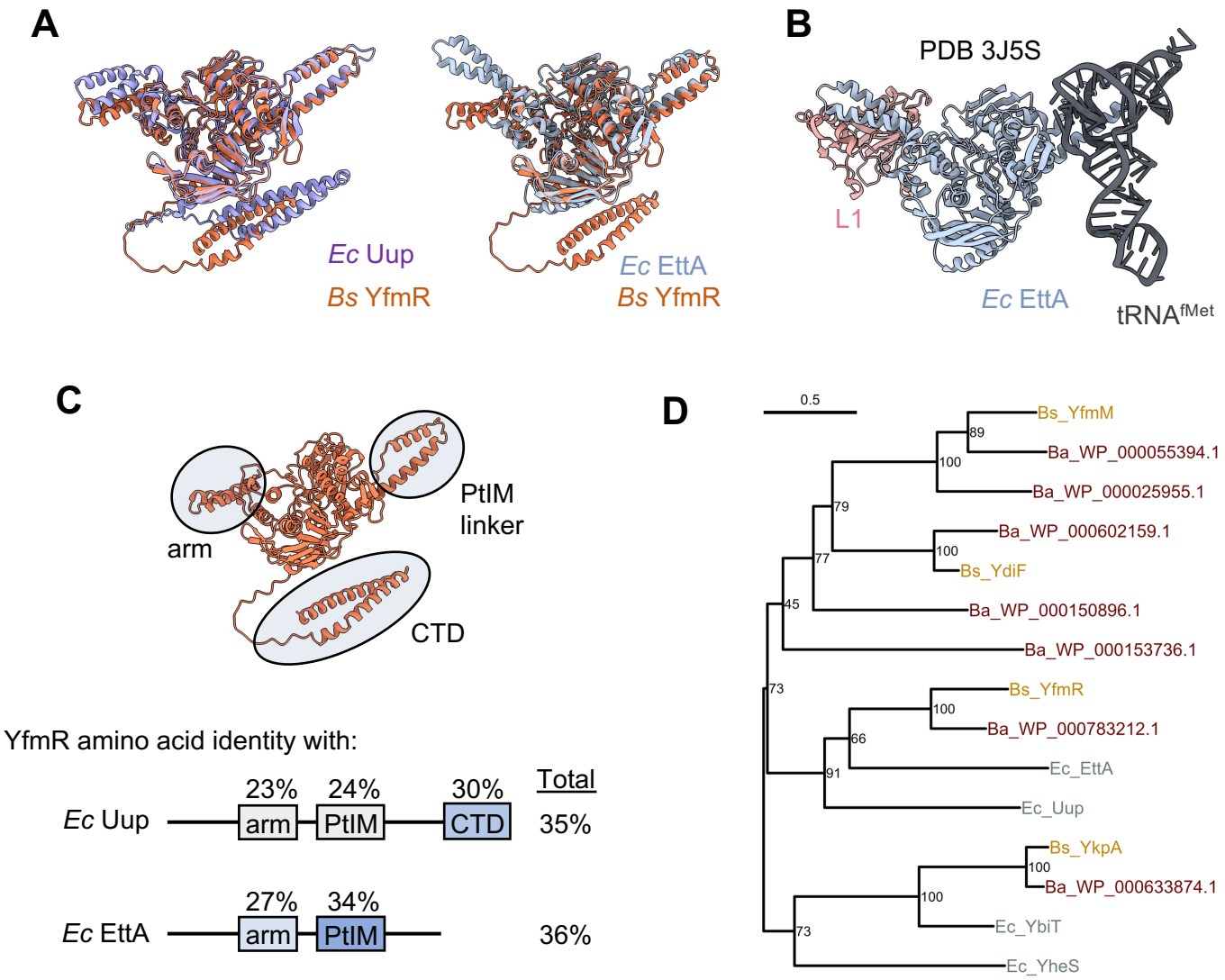

Fig 6. YfmR belongs to the Uup family of ABCFs but is more similar to EttA in the PtIM domain. (A) Overlay of the AlphaFold predicted structures of *B. subtilis* YfmR with *E. coli* Uup and EttA. All three proteins have a globular core containing 2 ATPase domains, and the arm and PtIM domains that contact the L1 stalk and the peptidyl-transferase-center, respectively. YfmR also encodes a C-terminal extension that is a defining feature of the Uup family. (B) Structure of *E. coli* EttA showing its contacts with the L1 stalk and the initiator $tRNA^{fMet}$ (PDB 3J5S). (C) Domain diagram showing sequence identity between *B. subtilis* YfmR and the arm, PtIM, and CTD of Uup and EttA. *B. subtilis* YfmR is 34% identical to EttA in the PtIM domain, which contacts the initiator $tRNA^{fMet}$. (D) Phylogenetic tree of amino acid sequences of ABCFs from *B. subtilis*, *B. anthracis* and *E. coli*. Numbers at nodes indicate maximum likelihood bootstrap percentage, which indicates likelihood of a common ancestor between the two branches.

S1

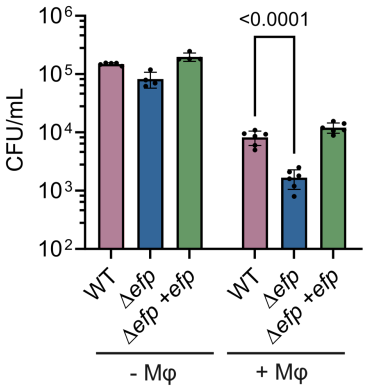

Fig S1. Δ*efp B. anthracis* is defective in survival in the presence of macrophages. J774A.1 macrophages (Mφ) were incubated with *B. anthracis* wild type and Δ*efp* cells for 2 hours at an MOI 0.1:1. Surviving bacteria were enumerated on LB agar plates. P-values are shown above brackets and were determined by an unpaired two-tailed T-test. Error bars represent standard deviation of 5 biological replicates.

S2

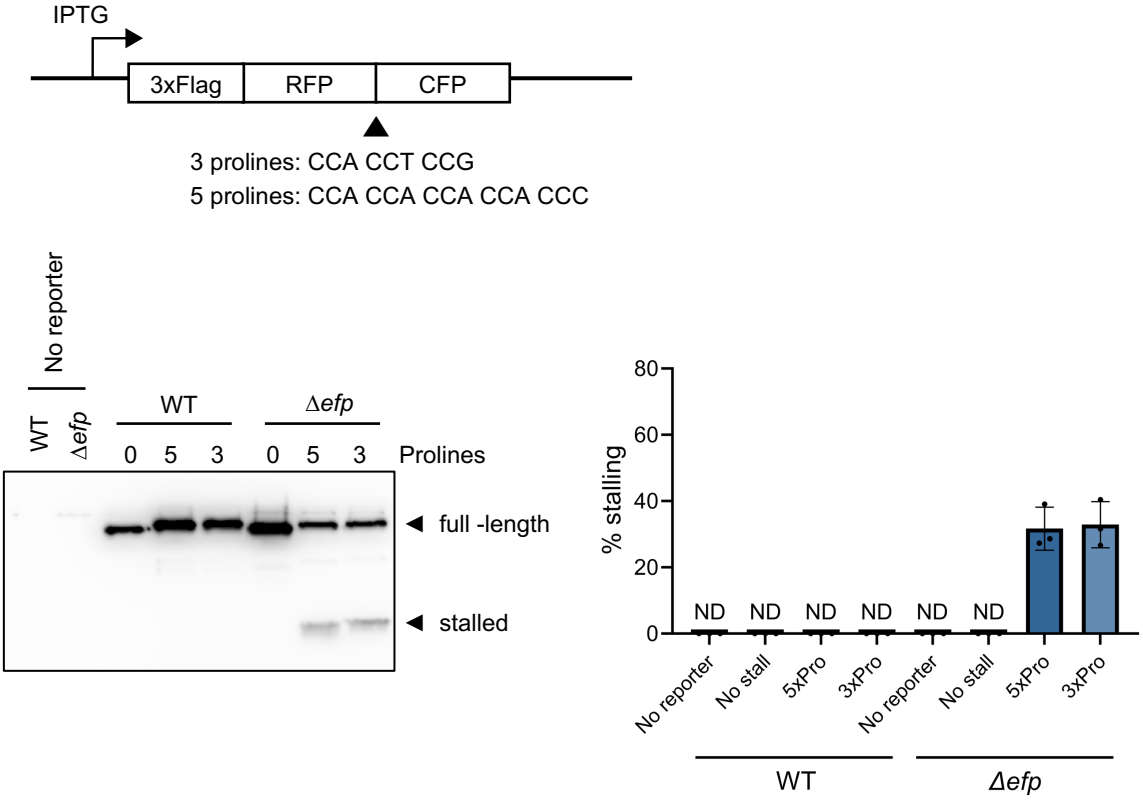

Fig S2. Measurement of ribosome stalling on polyproline motifs in *B. anthracis* wild type and Δ*efp*. A stalling reporter was constructed with three (CCA CCT CCG) or five (CCA CCA CCA CCA CCC) consecutive prolines in between an RFP and CFP fusion. The 3-proline stalling sequence is the motif from ValS (valyl-tRNA synthetase) of *B. anthracis.* Ribosome stalling at each motif was measured by western blot using anti-Flag antibody. Percent stalling was determined by measuring the ratio of stalled band intensity to total band intensity for both full-length and stalled peptide. Stalling levels were similar for both 3x prolines (32.9±7%) and 5x prolines (31.7±6.5 %). ND indicates not detectable. Error bars represent standard deviation of 3 biological replicates.

S3

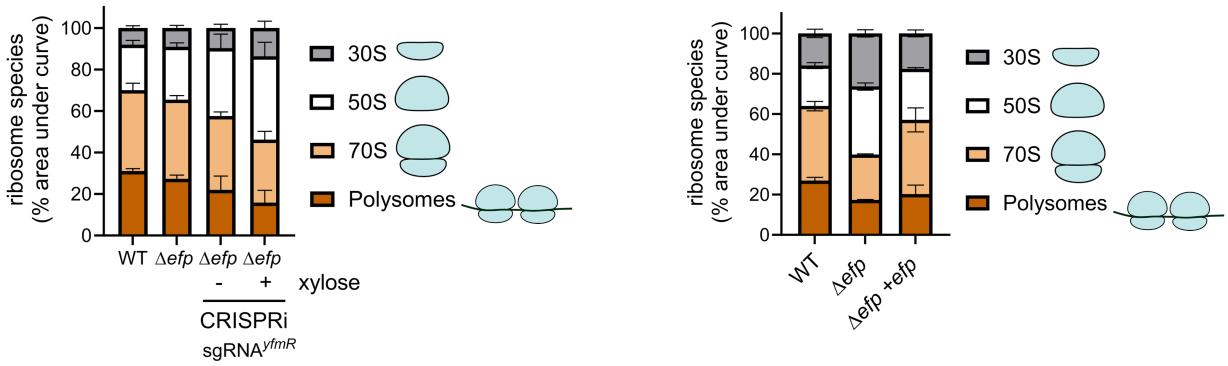

Fig S3. Quantification of relative levels of ribosome species separated by sucrose density gradient ultracentrifugation. Cleared lysates from *B. subtilis* wt, Δ*efp*, and Δ*efp* with dCas9+sgRNA^{yfmR} +/- xylose induction, as well as cleared lysates from *B. anthracis* wt, Δ*efp*, and Δ*efp* + *efp* integrated at *sacA* were separated on a 10%-40% sucrose density gradient. The relative abundance of each species was determined by taking the area under the curve for each peak and dividing by total area under the curve for the entire gradient. Error bars represent the standard deviation of 3 biological replicates.

S4

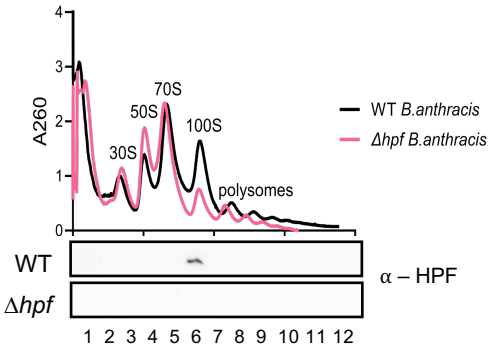

Fig S4. Confirmation that the 100S peak in log-phase *B. anthracis* contains HPF-bound ribosome dimers. HPF deletion eliminates the 100S peak and makes the first polysome peak visible. HPF is detected in the 100S peak with a polyclonal antibody raised against *B. subtilis* HPF.